

# The Confined $\beta$ -Soft rotor model in rare-earth nuclei

Jim A. Papadopoulos<sup>a,1</sup>, T.J. Mertzimekis<sup>a</sup>, P. Koseoglou<sup>a</sup>, P. Vasileiou<sup>a,2</sup>, Dennis Bonatsos<sup>b</sup>

<sup>a</sup>*National and Kapodistrian University of Athens, Zografou Campus, Athens, GR-15784, Greece*

<sup>b</sup>*Institute of Nuclear and Particle Physics, National Centre for Scientific Research "Demokritos", Aghia Paraskevi, Athens, GR-15310, Greece*

---

## Abstract

Contemporary theoretical descriptions of nuclear structure rely mainly on microscopic, single-particle frameworks often in competition with collective degrees of freedom, especially when deformation plays a dominant role. Such phenomena are prominent in the rare-earth region, where rotational band structures and enhanced electric quadrupole transitions are systematically examined. The Confined  $\beta$ -Soft (CBS) rotor model, introduced by N. Pietralla and O.M. Gorbachenko, bridges the gap between the X(5) critical point and the rigid-rotor limit in the region where the ratio  $R_{4/2} = E(4^+)/E(2^+)$  ratio lies between 2.904 and 3.333. In the present work, the CBS framework is employed to calculate ground-state band energies, associated B(E2) transition rates, and  $\beta$ -band excitations of even-even nuclei in the rare-earth region. The theoretical results are systematically compared with available experimental data, and predictions are provided for nuclear observables that have not yet been measured, offering guidance for future experimental investigations.

*Keywords:* CBS model, rare-earth, rigid-rotor, deformation

---

arXiv:2606.12264v1 [nucl-th] 10 Jun 2026

---

<sup>1</sup>Present address: Department of Physics, University of Guelph, Guelph, Ontario N1G 2W1, Canada

<sup>2</sup>Present address: Horia Hulubei National Institute of Physics and Nuclear Engineering - IFIN-HH, R-077125 Bucharest, Romania

## Contents

1. Introduction	3
2. The CBS Model	4
2.1. Theoretical framework	4
2.2. Methodology	7
3. Results and Discussion	8
3.1. Experimental data sources	8
3.2. General remarks	8
3.3. Ce (Z=58)	11
3.4. Nd (Z=60)	11
3.5. Sm (Z=62)	11
3.6. Gd (Z=64)	12
3.7. Dy (Z=66)	12
3.8. Er (Z=68)	13
3.9. Yb (Z=70)	13
3.10. Hf (Z=72)	14
3.11. W (Z=74)	14
3.12. Os (Z=76)	14
3.13. Identifying possible X(5) candidates	15
4. Conclusions	15
References	16
Explanation of Tables	40

## 1. Introduction

Structural characteristics in atomic nuclei are almost always not possible to be explained by the simple picture of a spherical nucleus. Indeed, in many regions of the nuclear chart, particularly among medium- and heavy-mass nuclei, an increasing number of valence nucleons leads to spontaneous breaking of spherical symmetry, resulting in deformed shapes [1]. This nuclear deformation has profound consequences for the structure and excitation modes of nuclei and also introduces considerable complexity in the theoretical description and prediction of the evolution of the nuclear structure. Deformed nuclei are typically associated with collective phenomena, where nucleons move coherently, giving rise to rotational bands and vibrational excitations that differ markedly from those found in spherical systems. Although collectivity has been extensively observed and studied for decades, its precise theoretical treatment remains an open challenge [2].

Modern single-particle and *ab initio* approaches, while powerful for light nuclei, struggle to describe collective motion in heavier systems due to the increasing number of active degrees of freedom [3, 4]. As a result, collective models continue to play a crucial role in describing the structure of nuclei in regions where deformation dominates. In this work, we focus on rare-earths (Ce to Yb) and a few heavier neighbors (Hf to Os), where nuclear structure evolves from near-spherical to highly deformed shapes. Since this region exhibits a broad range of quadrupole collectivity and includes some of the most deformed nuclei in the nuclear chart, it provides an excellent testing ground for collective models. Following Iachello's proposal for the symmetries E(5) and X(5) [5, 6], which describe the critical points of the shape phase transitions from spherical to  $\gamma$ -unstable nuclei and from spherical to axially deformed nuclei, respectively, numerous interpretations and extensions have emerged to predict excitation energies and quadrupole transition strengths associated with collective motion [7]. Among these, the Confined  $\beta$ -Soft (CBS) rotor model, introduced by Pietralla *et al.* [8, 9], provides a simple, yet effective, analytic solution of the Bohr Hamiltonian restricted to the axially symmetric case ( $\gamma \approx 0^\circ$ ), bridging the gap between the X(5) critical-point symmetry and the SU(3) limit (rigid rotor).

### *Motivation*

The CBS model provides predictions for both excitation energies and reduced electric quadrupole transition probabilities and is therefore well suited for a systematic study of collective nuclear structure. In the present work, we apply the model to even-even rare-earth nuclei with  $2.904 < R_{4/2} < 3.333$ , where  $R_{4/2} = E(4_1^+)/E(2_1^+)$ , corresponding to nuclei lying between the X(5) critical-point symmetry

and the rigid-rotor limit. This interval covers an important region of the nuclear chart where nuclei are well deformed and collective rotational motion dominates, whereas purely single-particle approaches become less effective. By focusing on this region, the CBS rotor model allows for a description of the collective behavior, using a relatively simple framework to study systematic trends across isotopic chains. At the same time, deviations from the model predictions can point to the presence of additional physical effects included in a non-purely collective description.

Moreover, a long-standing open problem in this mass region concerns the nature of excited  $0^+$  states and their interpretation as bandheads of the so-called  $\beta$ -bands [10–13], that is, rotational bands built on top of these states. Despite extensive experimental and theoretical studies exist, the structure and origin of these states still remain under debate [13].

In the above context, the CBS rotor model can be particularly useful, as it allows the simultaneous calculation of energy levels and quadrupole transition strengths, not only within the ground-state band, but for the  $\beta$ -band, as well. By applying the model systematically to rare-earth even–even nuclei, we aim to investigate the collective character and evolution of the excited  $0^+$  bandheads and the rotational bands built upon them. In this way, the present study may guide future experimental efforts toward targeted measurements of B(E2) transition strengths and excited  $0^+$  states, while also highlighting the limitations of purely collective models and pointing to missing physics that should be addressed in more refined theoretical approaches.

## 2. The CBS Model

### 2.1. Theoretical framework

We proceed to give a brief description of the CBS model. As already stated, the CBS rotor model interpolates between the X(5) limit, which corresponds to an analytical solution of the Bohr Hamiltonian [6], and the rigid-rotor limit, allowing the degree of  $\beta$ -softness to vary across this region. The interested reader can refer to references [8, 14] for the full details. The starting point for this model is the Bohr collective Hamiltonian [15–17]:

$$\hat{H} = -\frac{\hbar^2}{2B} \left[ \frac{1}{\beta^4} \frac{\partial}{\partial \beta} \left( \beta^4 \frac{\partial}{\partial \beta} \right) + \frac{1}{\beta^2 \sin 3\gamma} \frac{\partial}{\partial \gamma} \left( \sin 3\gamma \frac{\partial}{\partial \gamma} \right) - \frac{1}{4\beta^2} \sum_{k=1}^3 \frac{\hat{Q}_k^2}{\sin^2 \left( \gamma - \frac{2\pi k}{3} \right)} \right] + V(\beta, \gamma), \quad (1)$$

where  $\beta$  and  $\gamma$  denote the collective quadrupole deformation parameters [15, 18–20]. The parameter  $\beta$  describes the magnitude of the quadrupole deformation (deviation from sphericity), while  $\gamma$  characterizes the deviation of the nuclear shape from axial symmetry. Quantity  $B$  is the collective mass

parameter, and the operators  $\hat{Q}_k$  ( $k = 1, 2, 3$ ) represent the components of the angular momentum in the intrinsic frame. Eq. (1) corresponds to a five-dimensional Schrödinger equation which cannot be solved analytically unless specific simplifying approximations are introduced [5]. A major issue in solving the eigenvalue problem with Eq. (1) pertains to its non-separability, which can be overcome by considering a potential  $V(\beta, \gamma) = u(\beta) + v(\gamma)$  [6] for axially symmetric prolate ( $\gamma \approx 0^\circ$ ) nuclei. Then, the wave functions can be separated into

$$\Psi(\beta, \theta_i) = \xi_L(\beta) \mathcal{D}_{M,K}^L(\theta_i), \quad (2)$$

where  $\mathcal{D}_{M,K}^L$  are the Wigner functions and  $\theta_i$  the Euler angles of the intrinsic system. By focusing on the radial part of the Bohr–Hamiltonian, one gets

$$-\frac{\hbar^2}{2B} \left[ \frac{1}{\beta^4} \frac{\partial}{\partial \beta} \left( \beta^4 \frac{\partial}{\partial \beta} \right) - \frac{L(L+1)}{3\beta^2} + u(\beta) \right] \xi_L(\beta) = E \xi_L(\beta). \quad (3)$$

At this point, the Confined  $\beta$ -Soft rotor model can be applied. Unlike the X(5) solution, the CBS framework employs a potential well with a “moving wall” [7]

$$u(\beta) = \begin{cases} 0, & \text{for } \beta \in [\beta_m, \beta_M], \\ \infty, & \text{otherwise.} \end{cases} \quad (4)$$

which bridges the region between the X(5) critical point ( $\beta_m=0$ ) and the rigid rotor when  $\beta_m=\beta_M$  (1).

Inserting this potential in (3) leads to a Bessel equation of the form:

$$\tilde{\xi}'' + \frac{\tilde{\xi}'}{z} + \left( 1 - \frac{\nu^2}{z^2} \right) \tilde{\xi} = 0, \quad (5)$$

where  $z = \sqrt{\frac{E}{\hbar^2/2B}} \beta$ ,  $\tilde{\xi}(z) = \beta^{3/2} \xi_L(\beta)$  and  $\nu = \sqrt{\frac{L(L+1)}{3} + \frac{9}{4}}$ . Eq. (5) has solutions that are linear combinations of the Bessel functions  $J_\nu(z)$  and  $Y_\nu(z)$  of order  $\nu$ :

$$\tilde{\xi}_\nu(z) \propto A J_\nu(z) + B Y_\nu(z), \quad (6)$$

which can also be written as

$$\tilde{\xi}_\nu(z) \propto J_\nu(z) + \gamma Y_\nu(z) \quad (7)$$

where  $\gamma = \frac{B}{A}$ . Following the derivation in [8], one obtains the energy eigenvalues

$$E_{L,s} = \frac{\hbar^2}{2B} \left( \frac{z_{L,s}^{(r\beta)}}{\beta_M} \right)^2, \quad (8)$$

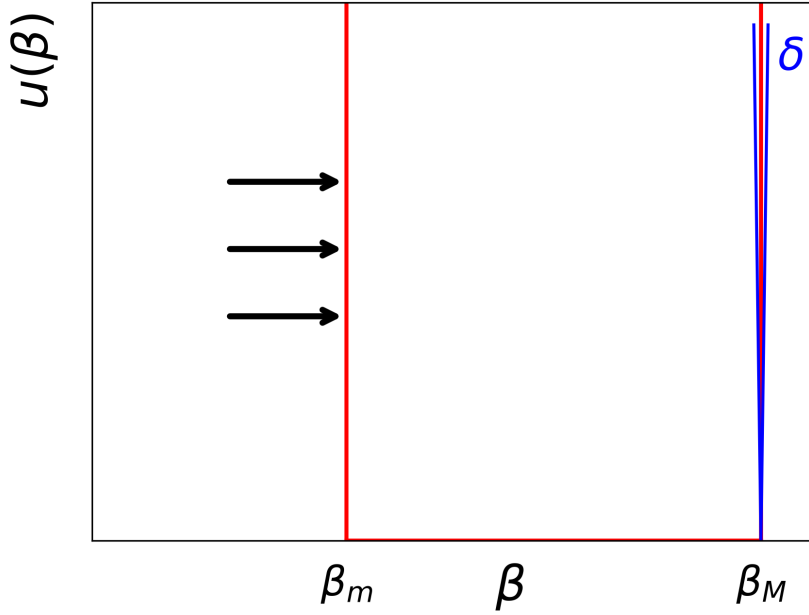


**Fig. 1:** The "moving wall" of the CBS potential, interpolating between the X(5) critical-point symmetry and the rigid-rotor limit.

where  $B$  denotes the mass parameter of the liquid drop model. An analytical description of the origin of this parameter can be found in [18, 20]. These eigenvalues depend on a single parameter,  $r_\beta$ , defined as:

$$r_\beta = \frac{\beta_m}{\beta_M}, \quad (9)$$

used to characterize the relative position of the inner and outer boundaries of the  $\beta$ -potential well. It defines the ratio of these boundaries and determines the stiffness of the  $\beta$  degree of freedom [8]. It also takes values in the interval  $0 \leq r_\beta \leq 1$ , with the limits  $r_\beta = 0$  and  $r_\beta = 1$  corresponding to the X(5) critical-point symmetry and the rigid-rotor limit, respectively. For each isotope,  $r_\beta$  can be determined by fitting the calculated ground-state energy ratios to the experimental ones. In practice, a trial value of  $r_\beta$  fixes the corresponding Bessel zeros  $z_{L,1}(r_\beta)$ , from which the normalized excitation energies are computed. The value of  $r_\beta$  is varied until the deviation between calculated and experimental ratios is minimized. Smaller  $r_\beta$  values produce softer, transitional behavior near the X(5) limit ( $R_{4/2} = 2.904$ ), whereas larger  $r_\beta$  correspond to a stiffer  $\beta$  potential approaching the rigid-rotor limit ( $R_{4/2} = 3.333$ ), associated with the SU(3) limit [21]. The CBS model was successfully used in the past to describe the even-even  $^{152-156}\text{Sm}$  [8] and  $^{150-156}\text{Nd}$  [14] isotopes analytically, showing the capabilities of the model. Moreover, regarding the calculation of the B(E2) transition strengths, the following E2 operator is

employed:

$$T_{\mu}^{\Delta K=0}(E2) = e^{(1)} \beta_M \langle \cos \gamma \rangle_{\gamma} \left( \frac{\beta}{\beta_M} \right) - \sqrt{\frac{2}{7}} e^{(2)} \beta_M \left[ \frac{\langle \cos 2\gamma \rangle_{\gamma}}{\langle \cos \gamma \rangle_{\gamma}} \left( \frac{\beta}{\beta_M} \right)^2 \right] D_{\mu 0}^2(\Omega), \quad (10)$$

which can be written as

$$T_{\mu}^{\Delta K=0}(E2) = e_{\text{eff}} \left[ \left( \frac{\beta}{\beta_M} \right) + \chi \left( \frac{\beta}{\beta_M} \right)^2 \right] D_{\mu 0}^2(\Omega), \quad (11)$$

with the effective charge

$$e_{\text{eff}} = e^{(1)} \beta_M \langle \cos \gamma \rangle_{\gamma} \quad (12)$$

and

$$\chi = -\sqrt{\frac{2}{7}} e^{(2)} \beta_M \frac{\langle \cos 2\gamma \rangle_{\gamma}}{\langle \cos \gamma \rangle_{\gamma}} \quad (13)$$

to be adjusted to available experimental B(E2) transition data [8]. Here,  $e^{(1)}$  and  $e^{(2)}$  denote the effective quadrupole charge parameters associated with the linear and quadratic terms of the collective E2 transition operator, respectively. Overall, it can be seen that the CBS rotor model uses only two dimensionless parameters,  $r_{\beta}$  and  $\chi$ , and two scale factors,  $\hbar^2/(2B\beta_M^2)$  and  $e_{\text{eff}}$ .

## 2.2. Methodology

This section describes the practical computational procedure followed to obtain numerical results within the CBS rotor model. The emphasis is placed on how the model is implemented and used in practice, rather than on its theoretical formulation, which has been fully described in the original publication [8]. The model starts by fitting on experimental excitation energies of the ground state band, at least up to the  $6_1^+$  state. In this work, we feed experimental excitation energies up to the  $8_1^+$  or, where available, the  $10_1^+$  state, to achieve the best possible determination of the  $r_{\beta}$  parameter. From this fit, the values of the parameter  $r_{\beta}$  and the energy scale factor  $B\beta_M^2$  can be obtained. The parameter  $r_{\beta}$  is determined by minimizing the weighted  $\chi^2$  (not to be confused with the parameter  $\chi$  in Eq. (13)):

$$\chi^2 = \sum_{I=2}^{I_{\text{max}}} \frac{(E(I_1^+)_{\text{exp}} - E(I_1^+; \text{CBS}))^2}{\sigma_{I,\text{exp}}^2}, \quad (14)$$

where the sum runs over the measured ground-state band energies from  $I = 2$  up to  $I_{\text{max}}$  (8 or 10, depending on data availability), and  $\sigma_{I,\text{exp}}$  is the experimental uncertainty on each level energy. This is handled internally by the CBS code [9].

Regarding the calculation of B(E2) transition strengths, we use the experimental values of  $B(E2; 2_1^+ \rightarrow 0_1^+)$  and  $B(E2; 4_1^+ \rightarrow 2_1^+)$ , where available, to determine the value of  $\beta_M$ . At this point it should be stressed

that, as stated in [22], while the CBS code enables either a constrained fit of  $\beta_M$  with fixed  $r_\beta$  and  $B\beta_M^2$ , or a simultaneous fit of all three parameters, both cases result in identical parameter values. We therefore choose to simultaneously fit all the parameters, as well as the  $\chi$  parameter and the scale factor  $e_{\text{eff}}$  in Eq. (11). Especially for the calculation of the energies, the following formula is employed [9]:

$$E(L, s) = \begin{cases} E_0 + \frac{z_{L,s}^2 - z_{0,s}^2}{2B\beta_{\text{max}}^2} + \epsilon L(L+1), & s = 1, \\ b_s(E(L, s) + b_s), & \text{else.} \end{cases} \quad (15)$$

### 3. Results and Discussion

In this section we proceed to list the literature sources from which the experimental data were obtained (Sec. 3.1), and give some general remarks regarding theoretical predictions (Sec. 3.2). Following that, a short discussion is presented for each individual isotopic chain under consideration (Sec. 3.3-3.12)

#### 3.1. Experimental data sources

Experimental excitation energies for the ground-state band were retrieved from the ENSDF (NUDAT) database [23] and from evaluated data compiled in Nuclear Data Sheets [24–46]. For the comparison of the model results for the reduced electric quadrupole transition probabilities  $B(E2)$ , we used the recommended values from the tables of E2 transition probabilities [47], supplemented by evaluated data from Nuclear Data Sheets [24, 25, 29–40, 42–46, 48]. In addition, a dedicated literature search was performed to identify recently published, non-evaluated experimental data [22, 49–55], which were also included in the present investigation.

#### 3.2. General remarks

The predictions for the excited energy states and  $B(E2)$  transition ratios of the ground-state band of even-even rare-earth nuclei up to the  $10^+$ , together with the corresponding experimental values, are presented in Tables A and B, respectively. Table C summarizes the excitation energies of the  $\beta$ -band up to the  $6^+$  state in keV, along with the corresponding quadrupole transition-strength ratios. Fig. 2 provides a systematic overview of the extracted  $r_\beta$  values for each isotope studied in the present work.

As seen in Table A, the CBS rotor model reproduces the ground-state band energies of even-even nuclei in the rare-earth region with high precision, showing the capability of the model to find a  $r_\beta$  value to fit well each of the isotopes examined in the region. This level of agreement is consistent

with the interpretation that even–even rare-earth nuclei exhibit strong quadrupole collectivity and relatively stable axial deformation, especially in their low-lying states. In this mass region, the low-lying excitation spectrum is dominated by rotational motion of a deformed intrinsic shape, and collectivity reduces the influence of single-particle degrees of freedom [17]. The CBS results presented in Table B show that the model reproduces the overall trend of the  $B(E2)$  transition ratios for the lowest excited states reasonably well, within the experimental uncertainties. In contrast, in many cases, the model fails to reproduce the observed systematics of these transition ratios at higher spins. Since this discrepancy cannot be attributed to a simple overall scaling, it suggests a deeper physical origin that warrants further investigation.

In particular, CBS predictions generally show smooth increasing ratios with angular momentum  $L$ , revealing a higher rigidity. The increase in the average deformation  $\langle\beta\rangle_L$  with angular momentum is referred to as centrifugal stretching and is caused by the  $L(L+1)$  centrifugal term in Eq. (3) [14, 56]. However, as shown in Table B, the experimental values do not always follow this monotonic trend. For example, some nuclei exhibit  $R_{6/2} < R_{4/2}$ ,  $R_{10/2} < R_{8/2}$ , or irregular jumps, such as:  $R_{4/2} = 1.559 \rightarrow R_{6/2} = 1.418 \rightarrow R_{8/2} = 1.856 \rightarrow R_{10/2} = 1.336$  (see  $^{162}\text{Yb}$ ). In many cases, experimental values for  $R_{10/2}$  drop after peaking around  $R_{6/2}$  or  $R_{8/2}$ . Such behavior is commonly associated with the onset of backbending, a well-known phenomenon in deformed nuclei whereby the moment of inertia increases abruptly with spin [57, 58]. Microscopically, backbending is interpreted as the alignment of high- $j$  quasiparticles –typically pairs of neutrons or protons– along the rotational axis [59]. This reflects the model assumption of persistent rigidity at higher angular momentum, which is not always valid in real nuclei. As a result, CBS predictions can overestimate the degree of rigidity, especially for large values of  $r_\beta$ , which correspond to stronger confinement in the  $\beta$ -degree of freedom. In such cases, the model tends to reproduce rigid-rotor-like behavior, while experimental data often reveal saturation or even a reduction in rigidity with increasing spin. Moreover, irregular changes in the experimental  $B(E2)$  ratios may suggest other phenomena not captured by the CBS framework, such as band crossings, configuration changes (e.g., alignment of an  $i_{13/2}$  neutron orbital) and mixing with non-yrast or two-quasiparticle states [60–62]. Since CBS is a purely collective model based on the Bohr Hamiltonian, it does not incorporate such microscopic effects [14]. While it provides useful insight into collective trends, its predictive power at high angular momentum is inherently limited. It should also be noted that the  $\gamma$  degree of freedom is not explicitly taken into account in the CBS model. In this framework, the potential  $V(\beta, \gamma)$  in Eq. (1) is minimized at  $\gamma \approx 0^\circ$ , corresponding to small harmonic oscillations

around axial symmetry. As a result, the model is effectively restricted to axially symmetric shapes and does not describe  $\gamma$ -softness. However, several works have shown that the  $\gamma$  degree of freedom can play an important role in the same regions of the nuclear chart (see, e.g., [63–65]). This limitation should therefore be kept in mind when interpreting the results presented in the plots and tables below.

Another important observation in Table B is the scarcity of experimental data for quadrupole transitions, particularly between higher-spin states. This underscores the need for new and precise measurements to better constrain theoretical models and improve our understanding of nuclear structure.

Regarding the CBS calculations of the excited  $0_{\beta}^{+}$  states in Table C, we observe the following correlation between the  $r_{\beta}$  parameter and the evolution of these states: for smaller values of  $r_{\beta}$  close to the X(5) limit, the potential in  $\beta$  is softer and thus the  $\beta$ -band appears at lower excitation energy, while in nuclei close to the rigid-rotor limit, where  $r_{\beta}$  approaches 1, the potential becomes narrow and stiff and this strong confinement of the  $\beta$ -motion results in a large restoring force, rapidly pushing the  $\beta$ -bandhead to higher excitation energies [8]. At the same time, Table C provides a useful set of predictions for the  $\beta_1$  band, which may assist in its identification among several experimentally observed excited  $K = 0^{+}$  bands in a given nucleus. Such identification is often nontrivial, as the nature of excited  $0^{+}$  states remains an open question: they may correspond to vibrational excitations about the deformed ground-state shape, to bandheads associated with coexisting shape minima, or to quasiparticle excitations [13]. Therefore, the present results may serve as a practical tool for the interpretation of experimental data and guidance for future studies.

Before discussing each isotopic chain separately, Fig. 2 provides an overall view of the  $r_{\beta}$  values for all the rare-earth nuclei examined in the present work. The parameter  $r_{\beta}$  has been shown to correlate with the ground-state band ratio  $R_{4/2}$  [8, 14], a trend that is also consistent with the evolution of the energy ratios displayed in Figs. 3–12. An interesting feature of Fig. 2 is the systematic evolution of the  $r_{\beta}$  values across the rare-earth region. The largest value is found for  $^{178}\text{Yb}$ , with  $r_{\beta} = 0.509$  [66], identifying it as the most rigidly deformed nucleus in the present set. More generally, the figure reveals a clear structural trend: as the proton number  $Z$  increases, the maximum of  $r_{\beta}$ , and hence the peak of rotational rigidity, shifts toward larger neutron number  $N$ . This shift of the maximum towards higher neutron number with increasing proton number reflects the need to maintain optimal quadrupole correlations [67].

### 3.3. Ce ( $Z=58$ )

For the Ce isotopic chain, Fig. 3 shows the evolution of the energy ratios  $E(I_1^+)/E(2_1^+)$  for Ce isotopes as a function of neutron number, separated into two regions ( $N \leq 70$  and  $N \geq 92$ ). The CBS calculations reproduce the overall experimental trends in both regions. In the lighter isotopes ( $N \leq 70$ ), a gradual decrease of the ratios with increasing neutron number is observed, indicating a reduction in rotational rigidity, which is consistently captured by the model. In contrast, for the heavier isotopes ( $N \geq 92$ ), the ratios increase with neutron number, reflecting a transition toward more rigid rotational behavior. It should also be noted that more neutron-rich isotopes, such as  $^{156}\text{Ce}$  and  $^{158}\text{Ce}$ , may also fall within the interval  $2.904 < R_{4/2} < 3.333$ , although no experimental data are currently available. Fig. 13 mainly highlights the scarcity of experimental results on quadrupole transition strengths in the Ce isotopic chain.

### 3.4. Nd ( $Z=60$ )

Similarly to the case of Ce isotopes, the experimental data for  $B(E2)$  transitions in Nd isotopes are rather limited, as seen in Fig. 14. Nevertheless, a noticeable decrease in the  $B(E2)$  ratios is observed between  $^{150}\text{Nd}$  ( $N = 90$ ) and  $^{152}\text{Nd}$  ( $N = 92$ ). Within the CBS framework, this behavior is correlated with the significant change in the  $r_\beta$  parameter, which increases from 0.098 for  $^{150}\text{Nd}$  to 0.382 for  $^{152}\text{Nd}$ . The higher  $r_\beta$  value for  $^{152}\text{Nd}$  indicates reduced  $\beta$ -softness and a tendency toward a more stabilized rotational structure, resulting in lower transition-strength ratios. This structural difference is also reflected in the energy systematics shown in Fig. 4, particularly for the higher-lying  $8_1^+$  and  $10_1^+$  states, where centrifugal stretching effects become more pronounced. It should also be noted that no experimental data are currently available for the  $8_1^+$  and  $10_1^+$  excited states of  $^{158}\text{Nd}$  in Fig. 4. Therefore, only the experimental energies up to  $6_1^+$  were used in the fit.

### 3.5. Sm ( $Z=62$ )

For Sm isotopes, the saturation of the energy ratios in Fig. 5 becomes evident beyond  $N = 104$  [68]. An important case is that of  $^{162}\text{Sm}$  ( $N = 100$ ), for which no experimental data are available for the  $6_1^+$  state of the ground-state band; consequently, a direct CBS fit could not be performed. To complete the isotopic chain, we estimated the energy of the  $6_1^+$  state. As a first step, we interpolated the  $6_1^+$  energy of  $^{162}\text{Sm}$  by averaging the  $R_{6/2}$  ratios of the neighboring isotopes  $^{160}\text{Sm}$  and  $^{164}\text{Sm}$ . The interpolated ratio for  $^{162}\text{Sm}$  is  $R_{6/2} = (6.830 + 6.770)/2 = 6.800$ . Multiplying by the experimental value of  $E_1^{2+}$  for  $^{162}\text{Sm}$ , we obtain  $E_1^{6+} = 485.5$  keV. However, this approach did not lead to a satisfactory CBS fit,

which is rather expected since a simple interpolation does not fully account for the structural evolution with neutron number. A more consistent approach is to use the  $R_{6/2}$  ratio of a nucleus whose  $R_{4/2}$  value is as close as possible to that of  $^{162}\text{Sm}$  ( $R_{4/2} = 3.304$ ). From Table A,  $^{172}\text{Yb}$  has  $R_{4/2} = 3.305$ , making it an excellent reference case. Using the corresponding  $R_{6/2}$  ratio, we obtain  $E_1^{6+} = 489.6$  keV, which leads to a successful CBS fit. In Fig. 15, experimental data are available only for  $^{152-154}\text{Sm}$ , where a relative agreement between the calculated and measured values is observed. For the remaining nuclei, we provide theoretical predictions within the CBS framework. Another interesting case is that of  $^{134}\text{Sm}$ . While it satisfies the condition  $2.904 < R_{4/2} < 3.333$ , the experimental data available in literature do not suffice for a successful fit by the CBS, suggesting the experimental data for this nucleus are worth revisiting in the near future.

### 3.6. Gd ( $Z=64$ )

Fig. 16 shows that  $^{154}\text{Gd}$  ( $N = 90$ ) and  $^{158}\text{Gd}$  ( $N = 94$ ) are well described by the CBS rotor model, as their  $B(E2)$  ratios follow the smooth increasing trend characteristic of collective rotational behavior. In Fig. 6, the CBS calculations reproduce the trend of the experimental energy ratios in the ground-state band, while also predicting values for the  $8_1^+$  and  $10_1^+$  excited states of  $^{164,166}\text{Gd}$ , for which no experimental data are currently available. A comparison with the available experimental data can also be made for  $^{156}\text{Gd}$  ( $N = 92$ ), where the CBS predictions lie close to the measured values, except for the  $B_{10/2}$  ratio, for which the model underestimates the transition strength. For  $^{160-166}\text{Gd}$ , no experimental data are currently available; therefore, the present results should be regarded as predictions of the CBS rotor model.

### 3.7. Dy ( $Z=66$ )

For the Dy isotopes, the CBS calculations shown in Fig. 7 reproduce the experimentally observed increase in rigidity with neutron number, reaching a maximum at  $N = 104$ . The saturation of the energy ratios with increasing neutron number is also evident, indicating stabilization of the nuclear deformation, as further addition of neutrons after  $N = 94$  does not significantly modify the collective structure. However, the same level of agreement between experiment and CBS predictions is not achieved regarding the  $B(E2)$ s, plotted in Fig. 17. Since transition rates are quite sensitive to the detailed structure and overlap of the wavefunctions, as well as to the specific form of the quadrupole operator,  $B(E2)$  observables probe finer structural features that are not entirely accounted for within the simplified CBS framework.

### 3.8. Er ( $Z=68$ )

In Fig. 8, saturation of the energy ratios of the ground-state band is once again observed, particularly in the region  $N = 100 - 104$ . Measurements of more neutron-rich Er isotopes would be of considerable interest in order to determine whether this saturation persists or whether the energy ratios decrease, indicating a deviation from rigid-rotor behavior and a possible re-emergence of single-particle effects influencing the ground-state deformation. In Fig. 18, many CBS predictions lie within the experimental uncertainties, or at least close to them, indicating the collective character of these transitions. However, as in most cases, the more neutron-rich Er isotopes, especially  $^{172}\text{Er}$  ( $N = 104$ ), lack experimental  $B(E2)$  data. The predicted trend may therefore serve as guidance for future experimental investigations. Finally, it should be noted that the  $B_{10/2}$  ratio for  $^{162}\text{Er}$  ( $N = 94$ ), recently measured by Kocheva *et al.* [22], is significantly lower than the general trend and suggests a possible onset of backbending. Such effects lie beyond the scope of the CBS rotor model, which does not account for quasiparticle alignments [14].

### 3.9. Yb ( $Z=70$ )

For the Yb isotopic chain, good agreement between the CBS predictions and the experimental ground-state band energies is once again observed in Fig. 9. The energy ratios exhibit a steady increase with neutron number  $N$  and reach a maximum at  $^{178}\text{Yb}$  ( $N = 108$ ,  $r_\beta=0.509$ ), reflecting the strengthening of rotational rigidity with increasing neutron number [66, 69]. It should be noted that the CBS calculation based on the experimental data available in the literature [41] yields a value of  $r_\beta = 0.496$ . However, as shown in Fig. 2, the use of the new measurements reported in [66] leads to  $r_\beta = 0.509$ , thereby establishing  $^{178}\text{Yb}$  as the most rigid nucleus in the rare-earth region. In addition, a substantial amount of experimental  $B(E2)$  data is available, allowing for systematic comparison. As shown in Fig. 19, most CBS predictions lie within the experimental uncertainties for the corresponding transition ratios. However, noticeable deviations are observed for  $^{168}\text{Yb}$  ( $N = 98$ ) in the  $B_{8/2}$  and  $B_{10/2}$  ratios, where the CBS model fails to reproduce the observed decrease in the  $B(E2)$  transition strengths. This drop suggests that the ground-state band is no longer purely collective at higher spin, and that single-particle degrees of freedom begin to play a more significant role. For  $^{178}\text{Yb}$ , no experimental  $B(E2)$  data are currently available, as lifetime measurements of the low-lying excited states in the ground-state band remain experimentally challenging [70].

### 3.10. Hf ( $Z=72$ )

In Fig. 10, a characteristic peak in the energy ratios is observed at  $N = 108$  ( $^{108}\text{Hf}$ ). For  $N = 108$ , the  $r_\beta$  parameter also reaches its highest value (0.463) within the Hf isotopic chain, indicating close proximity to the rigid-rotor limit. This maximum in rigidity at  $N = 108$  is also observed in the Yb, Hf, W, and Os isotopic chains, suggesting a systematic structural effect. As recently discussed [71],  $N = 108$  appears to act as a transition point where nuclei approach the SU(3) symmetry and subsequently evolve back toward the X(5) limit. This structural evolution is consistent with the observed decrease in the energy ratios beyond  $N = 108$ . For the  $B(E2)$  transitions, the CBS rotor model, following a purely collective approach, predicts a minimum of the  $B(E2)$  ratios at  $N = 108$ , in analogy with the peak observed in the energy ratios (see Fig. 20). However, the available experimental data do not fully support this behavior, with the exception of the low-lying  $B_{4/2}$  ratio. This deviation is not fully surprising, since quadrupole transition rates are influenced by additional structural effects, and single-particle degrees of freedom may play a non-negligible role, especially for transitions between higher energy levels.

### 3.11. W ( $Z=74$ )

Similarly to the behavior observed in the Hf isotopes, the energy ratios in the W isotopic chain exhibit a maximum at  $N = 108$ , indicating the end of the saturation, followed by a characteristic decrease (Fig. 11). In Fig. 21, the CBS calculations reproduce the overall experimental trends across all transitions, particularly for the  $4_1^+ \rightarrow 2_1^+$  and  $6_1^+ \rightarrow 4_1^+$  ratios. For higher-spin transitions ( $8_1^+ \rightarrow 6_1^+$  and  $10_1^+ \rightarrow 8_1^+$ ), the model continues to capture the general behavior, although some deviations are observed, especially at lower neutron numbers where experimental uncertainties are larger. The CBS predictions exhibit a smooth dependence on neutron number, indicating a gradual evolution of the rotational rigidity. A systematic investigation of W isotopes can be found in [71].

### 3.12. Os ( $Z=76$ )

The systematically smaller  $r_\beta$  parameters and lower  $R_{4/2}$  ratios observed in the W and Os isotopic chains (see Figs. 2, 11, and 12) can be attributed to their closer proximity to the  $Z = 82$  proton shell closure. As the proton number approaches the shell closure at  $Z = 82$ , the available valence space decreases, weakening the quadrupole interactions responsible for deformation. This suppresses the overall rigidity, which is reflected in reduced  $R_{4/2}$  ratios. Within the CBS framework, this structural effect is reflected in the smaller fitted values of the  $r_\beta$  parameter, indicating reduced rigidity compared

to e.g. Er and Yb. Additionally, Fig. 22 provides guidance for future experimental studies, as only limited experimental data are currently available for  $^{176-184}\text{Os}$ .

### 3.13. Identifying possible $X(5)$ candidates

This section aims to identify isotopes that may be described within the  $X(5)$  critical-point symmetry, namely nuclei located in the transitional region between spherical shapes and rigid rotors. Within the CBS interpretation, small values of the parameter  $r_\beta$  correspond to nuclei lying closer to the  $X(5)$  limit (see Fig. 2 and the related discussion). Among the nuclei traditionally discussed as possible  $X(5)$  candidates in the rare-earth region are  $^{150}\text{Nd}$ ,  $^{152}\text{Sm}$ ,  $^{154}\text{Gd}$ , and  $^{156}\text{Dy}$  [72, 73]. These nuclei belong to the well-known  $N = 90$  isotones, which are commonly associated with the spherical-to-axially-deformed phase-transitional region. In the present work, the corresponding fitted CBS values of  $r_\beta$  are found to be 0.098, 0.199, 0.203, and 0.139, respectively, further supporting their proximity to the  $X(5)$  limit. Moreover, several additional nuclei have been examined in the literature as possible  $X(5)$  candidates, such as  $^{128}\text{Ce}$ ,  $^{162}\text{Yb}$ ,  $^{166}\text{Hf}$ , and  $^{176}\text{Os}$ , with corresponding  $r_\beta$  values of 0.138, 0.036, 0.136, and 0.098, respectively [7, 74–76].

## 4. Conclusions

In the present work, a systematic study involving the CBS model was undertaken in the even-even isotopes from Ce ( $Z = 58$ ) to Os ( $Z = 76$ ). Ratios of level energies and reduced matrix elements, which generally serve as useful guides to understand structure evolution across the nuclear chart, have been calculated.

The results showcase the efficiency of the CBS model to describe the collective behavior of these nuclei in the ground-state and beta bands. They also highlight the existence of single-particle components in the wavefunction of some of these isotopes, stressing the need to expand the existing measurements to the outskirts of nuclear stability.

It is a core belief of the authors that the complete set of calculations presented in the tables and figures of this work may serve well researchers interested in exploring the nuclear structure properties in the rare-earth region. The results can be compared with predictions of other established models performing well in the same mass region (e.g. algebraic models) or be used to support future experimental endeavors. To that end, Table B highlights several missing  $B(E2)$  ratios, serving as a map to explore uncharted territories.

## Acknowledgments

PK acknowledges support by the DFG, Grant No 539757749.

## References

- [1] I. Hamamoto, B. Mottelson, Shape deformations in atomic nuclei, *Scholarpedia* 7 (2012) 10693. doi:[10.4249/scholarpedia.10693](https://doi.org/10.4249/scholarpedia.10693).
- [2] E. Litvinova, Recent advancements in the strongly coupled many-body problem, *arXiv* (2025). doi:[10.48550/arXiv.2512.23644](https://doi.org/10.48550/arXiv.2512.23644).
- [3] H. Hergert, A guided tour of *ab initio* nuclear many-body theory, *fphy* 8 (2020) 379. doi:[10.3389/fphy.2020.00379](https://doi.org/10.3389/fphy.2020.00379).
- [4] A. Ekström, C. Forssén, T. Papenbrock, et al., What is *ab initio* in nuclear theory?, *fphy* 11 (2023) 1129094. doi:[10.3389/fphy.2023.1129094](https://doi.org/10.3389/fphy.2023.1129094).
- [5] F. Iachello, Dynamic symmetries at the critical point, *Phys. Rev. Lett.* 85 (2000) 3580–3583. doi:[10.1103/PhysRevLett.85.3580](https://doi.org/10.1103/PhysRevLett.85.3580).
- [6] F. Iachello, Analytic description of critical point nuclei in a spherical-axially deformed shape phase transition, *Phys. Rev. Lett.* 87 (2001) 052502. doi:[10.1103/PhysRevLett.87.052502](https://doi.org/10.1103/PhysRevLett.87.052502).
- [7] P. Cejnar, J. Jolie, R. F. Casten, Quantum phase transitions in the shapes of atomic nuclei, *Rev. Mod. Phys.* 82 (2010) 2155–2212. doi:[10.1103/RevModPhys.82.2155](https://doi.org/10.1103/RevModPhys.82.2155).
- [8] N. Pietralla, O. M. Gorbachenko, Evolution of the “ $\beta$  excitation” in axially symmetric transitional nuclei, *Phys. Rev. C* 70 (2004, 011304). doi:[10.1103/PhysRevC.70.011304](https://doi.org/10.1103/PhysRevC.70.011304).
- [9] M. Reese, CBS model program, <https://sourceforge.net/projects/cbsmodel/>, 2011.
- [10] P. E. Garrett, Characterization of the  $\beta$  vibration and  $0_2^+$  states in deformed nuclei, *Journal of Physics G: Nuclear and Particle Physics* 27 (2001) R1–R29. URL: <https://doi.org/10.1088/0954-3899/27/1/201>. doi:[10.1088/0954-3899/27/1/201](https://doi.org/10.1088/0954-3899/27/1/201).
- [11] J. Sharpey-Schafer, R. Bark, S. Bvumbi, E. Lawrie, J. Lawrie, T. Madiba, S. Majola, A. Minkova, S. Mullins, P. Papka, D. Roux, J. Timár, A double vacuum, configuration dependent pairing and lack of  $\beta$ -vibrations in transitional nuclei: Band structure of  $n = 88$  to  $n = 91$  nuclei, *Nuclear Physics A* 834 (2010) 45c–49c. URL: <https://www.sciencedirect.com/science/article/>

- [pii/S0375947410000151](https://doi.org/10.1016/j.nuclphysa.2010.01.014). doi:<https://doi.org/10.1016/j.nuclphysa.2010.01.014>, the 10th International Conference on Nucleus-Nucleus Collisions (NN2009).
- [12] J. Sharpey-Schafer, R. Bark, S. Bvumbi, T. Dinoko, S. Majola, “stiff” deformed nuclei, configuration dependent pairing and the  $\beta$  and  $\gamma$  degrees of freedom, *The European Physical Journal A* 55 (2019) 15.
- [13] A. Aprahamian, K. Lee, S. R. Lesher and R. Bijker, The nature of  $0^+$  excitations in deformed nuclei, *Progress in Particle and Nuclear Physics* 143 (2025, 104173). doi:[10.1016/j.pnnp.2025.104173](https://doi.org/10.1016/j.pnnp.2025.104173).
- [14] K. Dusling, N. Pietralla, Description of ground-state band energies in well-deformed even-even nuclei with the confined  $\beta$ -soft rotor model, *Phys. Rev. C* 72 (2005) 011303. doi:[10.1103/PhysRevC.72.011303](https://doi.org/10.1103/PhysRevC.72.011303).
- [15] A. Bohr, *The Coupling of Nuclear Surface Oscillations to the Motion of Individual Nucleons*, Det Kgl. Danske Videnskabernes Selskab. Matematisk-fysiske meddelelser, Komm. Munksgaard, 1952. URL: <https://books.google.gr/books?id=A8QTtQEACAAJ>.
- [16] A. Bohr, B. R. Mottelson, *Nuclear Structure*, World Scientific, New York, 1997.
- [17] A. Bohr, B. Mottelson, *Nuclear Structure, Volume II: Nuclear Deformations*, W.A. Benjamin, 1975.
- [18] L. Fortunato, Solutions of the Bohr Hamiltonian, a compendium, *Eur. Phys. J. A* 26S1 (2005) 1–30. doi:[10.1140/epjad/i2005-07-115-8](https://doi.org/10.1140/epjad/i2005-07-115-8). arXiv:[nucl-th/0411087](https://arxiv.org/abs/nucl-th/0411087).
- [19] D. Bonatsos, P. E. Georgoudis, D. Lenis, N. Minkov, C. Quesne, Bohr hamiltonian with a deformation-dependent mass term for the davidson potential, *Phys. Rev. C* 83 (2011). doi:[10.1103/physrevc.83.044321](https://doi.org/10.1103/physrevc.83.044321).
- [20] P. Baganu, L. Fortunato, Recent approaches to quadrupole collectivity: models, solutions and applications based on the bohr hamiltonian, *Journal of Physics G: Nuclear and Particle Physics* 43 (2016) 093003. URL: <https://doi.org/10.1088/0954-3899/43/9/093003>. doi:[10.1088/0954-3899/43/9/093003](https://doi.org/10.1088/0954-3899/43/9/093003).
- [21] J. A. Papadopoulos, T. J. Mertzimekis, P. Koseoglou, D. Bonatsos, P. Vasileiou, M. Efstathiou, Investigation of the Yb and W Isotopic Chains using the Confined  $\beta$ -Soft Rotor Model, *HNPS Adv. Nucl. Phys.* 32 (2026) 107–112. doi:[10.12681/hnpsanp.8764](https://doi.org/10.12681/hnpsanp.8764).

- [22] D. Kocheva, K. A. Gladnishki, A. Blazhev, et al., Lifetimes and electromagnetic transition strengths in Er, *Eur. Phys. J. A* 62 (2026) 18. doi:[10.1140/epja/s10050-025-01778-0](https://doi.org/10.1140/epja/s10050-025-01778-0).
- [23] NUDAT, National Nuclear Data Center, online. <https://www.nndc.bnl.gov/nudat3/>.
- [24] S. Basu, A. Sonzogni, Nuclear Data Sheets for  $A=150$ , *Nucl. Data Sheets* 114 (2013) 435–660. doi:[10.1016/j.nds.2013.04.001](https://doi.org/10.1016/j.nds.2013.04.001).
- [25] M. Martin, Nuclear Data Sheets for  $A=152$ , *Nucl. Data Sheets* 114 (2013) p. 1497–1847. doi:[10.1016/j.nds.2013.11.001](https://doi.org/10.1016/j.nds.2013.11.001).
- [26] N. Nica, Nuclear Data Sheets for  $A=154$ , *Nuclear Data Sheets* 200 (2025) 2–524. URL: <https://www.sciencedirect.com/science/article/pii/S0090375225000134>. doi:<https://doi.org/10.1016/j.nds.2025.02.002>.
- [27] H. Iimura, J. Katakura, S. Ohya, Nuclear data sheets for  $a=126$ , *Nucl. Data Sheets* 180 (2022) 1–413. doi:<https://doi.org/10.1016/j.nds.2022.02.001>.
- [28] Z. Elekes, J. Timar, Nuclear data sheets for  $a = 128$ , *Nuclear Data Sheets* 129 (2015) 191–436. URL: <https://www.sciencedirect.com/science/article/pii/S0090375215000472>. doi:<https://doi.org/10.1016/j.nds.2015.09.002>.
- [29] C. Reich, Nuclear Data Sheets for  $A=156$ , *Nucl. Data Sheets* 113 (2012) 2537–2840. doi:[10.1016/j.nds.2012.10.003](https://doi.org/10.1016/j.nds.2012.10.003).
- [30] N. Nica, Nuclear Data Sheets for  $A=158$ , *Nucl. Data Sheets* 141 (2017) 1–326. doi:[10.1016/j.nds.2017.03.001](https://doi.org/10.1016/j.nds.2017.03.001).
- [31] N. Nica, Nuclear Data Sheets for  $A=160$ , *Nucl. Data Sheets* 176 (2021) 1–428. doi:[10.1016/j.nds.2021.08.001](https://doi.org/10.1016/j.nds.2021.08.001).
- [32] N. Nica, Nuclear Data Sheets for  $A=162$ , *Nucl. Data Sheets* 195 (2024) 1–367. doi:[10.1016/j.nds.2024.04.001](https://doi.org/10.1016/j.nds.2024.04.001).
- [33] B. Singh, J. Chen, Nuclear Data Sheets for  $A=164$ , *Nucl. Data Sheets* 147 (2018). doi:[10.1016/j.nds.2018.01.001](https://doi.org/10.1016/j.nds.2018.01.001).
- [34] C. M. Baglin, Nuclear Data Sheets for  $A=166$ , *Nucl. Data Sheets* 109 (2008) 1103–1382. doi:[10.1016/j.nds.2008.04.001](https://doi.org/10.1016/j.nds.2008.04.001).
- [35] C. M. Baglin, Nuclear Data Sheets for  $A=168$ , *Nucl. Data Sheets* 111 (2010) 1807 – 2080. doi:[10.1016/j.nds.2010.07.001](https://doi.org/10.1016/j.nds.2010.07.001).

- [36] C. Baglin, E. McCutchan, S. Basunia, E. Browne, Nuclear Data Sheets for  $A=170$ , Nucl. Data Sheets 153 (2018) 1–494. doi:[10.1016/j.nds.2018.11.001](https://doi.org/10.1016/j.nds.2018.11.001).
- [37] B. Singh, Nuclear Data Sheets for  $A=172$ , Nucl. Data Sheets 75 (1995) 199 – 376. doi:[10.1006/ndsh.1995.1025](https://doi.org/10.1006/ndsh.1995.1025).
- [38] M. Basunia, Nuclear Data Sheets for  $A=176$ , Nucl. Data Sheets 107 (2006) p. 791–1026. doi:[10.1016/j.nds.2006.03.001](https://doi.org/10.1016/j.nds.2006.03.001).
- [39] E. Achterberg, O. A. Capurro, G. V. Marti, Nuclear Data Sheets for  $A=178$ , Nucl. Data Sheets 110 (2009) 1473 – 1688. doi:[10.1016/j.nds.2009.05.002](https://doi.org/10.1016/j.nds.2009.05.002).
- [40] E. A. McCutchan, Nuclear Data Sheets for  $A=180$ , Nucl. Data Sheets 126 (2015) 151 – 372. doi:[10.1016/j.nds.2015.05.002](https://doi.org/10.1016/j.nds.2015.05.002).
- [41] E. Achterberg, O. Capurro, G. Marti, Nuclear Data Sheets for  $A=178$ , Nucl. Data Sheets 110 (2009) 1473–1688. doi:[10.1016/j.nds.2009.05.002](https://doi.org/10.1016/j.nds.2009.05.002).
- [42] B. Singh, Nuclear Data Sheets for  $A=182$ , Nucl. Data Sheets 130 (2015) 21–126. doi:[10.1016/j.nds.2015.11.002](https://doi.org/10.1016/j.nds.2015.11.002).
- [43] C. M. Baglin, Nuclear Data Sheets for  $A=184$ , Nucl. Data Sheets 111 (2010) 275–523. doi:[10.1016/j.nds.2010.01.001](https://doi.org/10.1016/j.nds.2010.01.001).
- [44] J. Batchelder, A. Hurst, M. Basunia, Nuclear Data Sheets for  $A=186$ , Nucl. Data Sheets 183 (2022) 1–346. doi:[10.1016/j.nds.2022.06.001](https://doi.org/10.1016/j.nds.2022.06.001).
- [45] F. Kondev, S. Juutinen, D. Hartley, Nuclear Data Sheets for  $A=188$ , Nucl. Data Sheets 150 (2018) 1–364. doi:[10.1016/j.nds.2018.05.001](https://doi.org/10.1016/j.nds.2018.05.001).
- [46] B. Singh, J. Chen, Nuclear Data Sheets for  $A=190$ , Nucl. Data Sheets 169 (2020) 1–390. doi:[10.1016/j.nds.2020.10.001](https://doi.org/10.1016/j.nds.2020.10.001).
- [47] B. Pritychenko, M. Birch, B. Singh, M. Horoi, Tables of E2 transition probabilities from the first  $2+$  states in even–even nuclei, At. Data Nucl. Data Tables 107 (2016) 1–139. doi:[10.1016/j.adt.2015.10.001](https://doi.org/10.1016/j.adt.2015.10.001).
- [48] C. W. Reich, Nuclear Data Sheets for  $A=154$ , Nucl. Data Sheets 110 (2009) 2257–2532. doi:[10.1016/j.nds.2009.09.001](https://doi.org/10.1016/j.nds.2009.09.001).
- [49] R. L. Canavan, M. Rudigier, P. H. Regan, M. Lebois, J. N. Wilson, N. Jovancevic, P.-A. Söderström, S. M. Collins, D. Thisse, J. Benito, S. Bottoni, M. Brunet, N. Cieplicka-Oryńczak,

- S. Courtin, D. T. Doherty, L. M. Fraile, K. Hadyńska-Klęk, G. Häfner, M. Heine, L. W. Iskra, V. Karayonchev, A. Kennington, P. Koseoglou, G. Lotay, G. Lorusso, M. Nakhostin, C. R. Niță, S. Oberstedt, Z. Podolyák, L. Qi, J.-M. Régis, V. Sánchez-Tembleque, R. Shearman, V. Vedia, W. Witt, Half-life measurements in  $^{164,166}\text{Dy}$  using  $\gamma$ - $\gamma$  fast-timing spectroscopy with the  $\nu$ -ball spectrometer, *Phys. Rev. C* 101 (2020) 024313. doi:[10.1103/PhysRevC.101.024313](https://doi.org/10.1103/PhysRevC.101.024313).
- [50] P. Petkov, A. Dewald, O. Möller, I. Deloncle, R. Chapman, S. Pascu, D. Bucurescu, D. Tonev, M. Reese, C. Fransen, S. Araddad, G. Asova, J. Copnell, N. Goutev, M. Hackstein, J. Jolie, J. Lisle, J. Mo, T. Pissulla, W. Rother, A. Smith, C. Tenreiro, D. Thompson, K. Zell, On the quadrupole collectivity in the yrast band of  $^{168}\text{Yb}$ , *Nucl. Phys. A* 957 (2017) 240–258. doi:[10.1016/j.nuclphysa.2016.09.006](https://doi.org/10.1016/j.nuclphysa.2016.09.006).
- [51] V. Karayonchev, J.-M. Régis, J. Jolie, A. Blazhev, R. Altenkirch, S. Ansari, M. Dannhoff, F. Diel, A. Esmaylzadeh, C. Fransen, R.-B. Gerst, K. Moschner, C. Müller-Gatermann, N. Saed-Samii, S. Stegemann, N. Warr, K. O. Zell, Evolution of collectivity in the  $n = 100$  isotones near  $^{170}\text{Yb}$ , *Phys. Rev. C* 95 (2017) 034316. doi:[10.1103/PhysRevC.95.034316](https://doi.org/10.1103/PhysRevC.95.034316).
- [52] M. Rudigier, K. Nomura, M. Dannhoff, R.-B. Gerst, J. Jolie, N. Saed-Samii, S. Stegemann, J.-M. Régis, L. M. Robledo, R. Rodríguez-Guzmán, A. Blazhev, C. Fransen, N. Warr, K. O. Zell, Evolution of E2 transition strength in deformed hafnium isotopes from new measurements on  $^{172}\text{Hf}$ ,  $^{174}\text{Hf}$ , and  $^{176}\text{Hf}$ , *Phys. Rev. C* 91 (2015) 044301. doi:[10.1103/PhysRevC.91.044301](https://doi.org/10.1103/PhysRevC.91.044301).
- [53] J. Wiederhold, V. Werner, R. Kern, N. Pietralla, D. Bucurescu, R. Carroll, N. Cooper, T. Daniel, D. Filipescu, N. Florea, R.-B. Gerst, D. Ghita, L. Gurgi, J. Jolie, R. S. Ilieva, R. Lica, N. Marginean, R. Marginean, C. Mihai, I. O. Mitu, F. Naqvi, C. Nita, M. Rudigier, S. Stegemann, S. Pascu, P. H. Regan, Evolution of E2 strength in the rare-earth isotopes  $^{174,176,178,180}\text{Hf}$ , *Phys. Rev. C* 99 (2019) 024316. doi:[10.1103/PhysRevC.99.024316](https://doi.org/10.1103/PhysRevC.99.024316).
- [54] A. Harter, L. Knafla, G. Frießner, G. Häfner, J. Jolie, A. Blazhev, A. Dewald, F. Dunkel, A. Esmaylzadeh, C. Fransen, V. Karayonchev, K. Lawless, M. Ley, J.-M. Régis, K. O. Zell, Lifetime measurements in the tungsten isotopes  $^{176,178,180}\text{W}$ , *Phys. Rev. C* 106 (2022) 024326. doi:[10.1103/PhysRevC.106.024326](https://doi.org/10.1103/PhysRevC.106.024326).
- [55] A. Harter, A. Esmaylzadeh, L. Knafla, C. Fransen, F. v. Spee, J. Jolie, M. Ley, V. Karayonchev, J. Fischer, A. Pfeil, Lifetime measurements in low yrast states and spectroscopic peculiarities in  $^{182}\text{Os}$ , *Phys. Rev. C* 108 (2023) 024305. doi:[10.1103/PhysRevC.108.024305](https://doi.org/10.1103/PhysRevC.108.024305).

- [56] A. Costin, M. Reese, H. Ai, R. F. Casten, K. Dusling, C. R. Fitzpatrick, G. Gürdal, A. Heinz, E. A. McCutchan, D. A. Meyer, O. Möller, P. Petkov, N. Pietralla, J. Qian, G. Rainovski, V. Werner, Centrifugal stretching along the ground state band of  $^{168}\text{Hf}$ , *Phys. Rev. C* 79 (2009) 024307. doi:[10.1103/PhysRevC.79.024307](https://doi.org/10.1103/PhysRevC.79.024307).
- [57] F. Stephens, R. Simon, Coriolis effects in the yrast states, *Nucl. Phys. A* 183 (1972) 257–284. doi:[10.1016/0375-9474\(72\)90658-6](https://doi.org/10.1016/0375-9474(72)90658-6).
- [58] R. Wyss, M. A. Riley, Fifty years of backbending, *Nucl. Phys. News* 32 (2022) 16–20. doi:[10.1080/10619127.2022.2063000](https://doi.org/10.1080/10619127.2022.2063000). arXiv:[10.1080/10619127.2022.2063000](https://arxiv.org/abs/10.1080/10619127.2022.2063000).
- [59] P. Ring, P. Schuck, *The Nuclear Many-Body Problems*, volume 103, Springer, 1980. doi:[10.1063/1.2915762](https://doi.org/10.1063/1.2915762).
- [60] F. S. Stephens, R. S. Simon, Properties of rotational bands in heavy nuclei, *Nucl. Phys. A* 183 (1972) 257–270. doi:[10.1016/0375-9474\(72\)90619-4](https://doi.org/10.1016/0375-9474(72)90619-4).
- [61] F. S. Stephens, Phenomena associated with the rotational alignment of nucleons, *Rev. Mod. Phys.* 47 (1975) 43–65. doi:[10.1103/RevModPhys.47.43](https://doi.org/10.1103/RevModPhys.47.43).
- [62] R. Bengtsson, S. Frauendorf, Rotational bands and particle alignment, *Nucl. Phys. A* 327 (1979) 139–160. doi:[10.1016/0375-9474\(79\)90509-8](https://doi.org/10.1016/0375-9474(79)90509-8).
- [63] P. Koseoglou, V. Werner, N. Pietralla, D. Bonatsos,  $N=90$  QSPT: Cerium, neodymium and samarium isotopic chains in the IBM symmetry triangle, *HNPS Adv. Nucl. Phys.* 26 (2019) 37–43. doi:[10.12681/hnps.1793](https://doi.org/10.12681/hnps.1793).
- [64] P. Koseoglou, V. Werner, N. Pietralla, S. Ilieva, T. Nikšić, D. Vretenar, P. Alexa, M. Thürauf, C. Bernardis, A. Blanc, A. M. Bruce, R. B. Cakirli, N. Cooper, L. M. Fraile, G. de France, M. Jentschel, J. Jolie, U. Köster, W. Korten, T. Kröll, S. Lalkovski, H. Mach, N. Mărginean, P. Mutti, Z. Patel, V. Pazyi, Z. Podolyák, P. H. Regan, J.-M. Régis, O. J. Roberts, N. Saed-Samii, G. S. Simpson, T. Soldner, C. A. Ur, W. Urban, D. Wilmsen, E. Wilson, Low- $Z$  boundary of the  $N = 88$ – $90$  shape phase transition:  $^{148}\text{Ce}$  near the critical point, *Phys. Rev. C* 101 (2020) 014303. doi:[10.1103/PhysRevC.101.014303](https://doi.org/10.1103/PhysRevC.101.014303).
- [65] P. Koseoglou, V. Werner, N. Pietralla,  $N = 90$  shape phase transition: increasing axial asymmetry towards  $^{148}\text{Ce}$ , *Bulg. J. Phys.* 49 (2022) p. 89–96.
- [66] P. Koseoglou, et al., 2026. (in preparation).

- [67] R. F. Casten, Empirical proton-neutron interaction and its relation to nuclear collectivity, *Phys. Rev. Lett.* 54 (1985) 1991–1994.
- [68] D. H. Feng, C.-L. Wu, M. W. Guidry, Z.-P. Li, Dynamical Pauli effects and the saturation of nuclear collectivity, *Phys. Lett. B* 205 (1988) 156–162. doi:[10.1016/0370-2693\(88\)91639-5](https://doi.org/10.1016/0370-2693(88)91639-5).
- [69] P. Koseoglou, T. J. Mertzimekis, M. Efstathiou, P. Vasileiou, H. Mayr, C. M. Nickel, N. Pietralla, V. Werner, A. Blazhev, A. Esmaylzadeh, J. Fischer, C. Fransen, J. Jolie, M. Ley, A. Pfeil, F. von Spee, K. Gladnishki, D. Kocheva, G. Rainovski, N. Florea, A. Radu, D. Tofan, D. Bonatsos, K. E. Karakatsanis, Gamma-spectrometry on the well-deformed  $^{178}\text{Yb}$ : excitation functions, *HNPS Adv. Nucl. Phys.* 32 (2026) 119–125. doi:[10.12681/hnpsanp.9053](https://doi.org/10.12681/hnpsanp.9053).
- [70] A. Zyriliou, et al., Nuclear Structure Investigations in Yb isotopes, *HNPS Adv. Nucl. Phys.* 28 (2022) 104–108. doi:[10.12681/hnps.3609](https://doi.org/10.12681/hnps.3609).
- [71] J. Gupta, V. Katoch, Review of nuclear structure  $N=86$ – $118$  of W isotopes, *Nucl. Phys. A* 1057 (2025, 123032). doi:[10.1016/j.nuclphysa.2025.123032](https://doi.org/10.1016/j.nuclphysa.2025.123032).
- [72] M. A. Caprio, Structure of collective modes in transitional and deformed nuclei, arXiv: Nuclear Experiment (2005). URL: <https://api.semanticscholar.org/CorpusID:119368092>.
- [73] J. B. Gupta, J. H. Hamilton, Outstanding problems in the band structures of  $^{152}\text{Sm}$ , *Phys. Rev. C* 96 (2017) 034321. doi:[10.1103/PhysRevC.96.034321](https://doi.org/10.1103/PhysRevC.96.034321).
- [74] Balabanski et al., Evidence for  $x(5)$  critical point symmetry in  $^{128}\text{Ce}$ , *International Journal of Modern Physics E* 15 (2012). doi:[10.1142/S0218301306005538](https://doi.org/10.1142/S0218301306005538).
- [75] D. Tonev, A. Dewald, T. Klug, P. Petkov, J. Jolie, A. Fitzler, O. Möller, S. Heinze, P. von Brentano, R. F. Casten, Transition probabilities in  $^{154}\text{Gd}$ : Evidence for  $X(5)$  critical point symmetry, *Phys. Rev. C* 69 (2004) 034334. doi:[10.1103/PhysRevC.69.034334](https://doi.org/10.1103/PhysRevC.69.034334).
- [76] E. Mccutchan, N. Zamfir, M. Caprio, R. Casten, H. Amro, C. Beausang, D. Brenner, A. Hecht, C. Hutter, S. Langdown, D. Meyer, P. Regan, J. Ressler, A. Yamamoto, Low spin states in  $^{162}\text{Yb}$  and the  $X(5)$  critical point symmetry, *Phys. Rev. C* 69 (2004). doi:[10.1103/PhysRevC.69.024308](https://doi.org/10.1103/PhysRevC.69.024308).
- [77] B. Singh, J. Chen, Nuclear Data Sheets for  $A=164$ , *Nucl. Data Sheets* 147 (2018) 1–381. doi:[10.1016/j.nds.2018.01.001](https://doi.org/10.1016/j.nds.2018.01.001).
- [78] B. Singh, Nuclear Data Sheets for  $A=172$ , *Nucl. Data Sheets* 75 (1995) 199–376. doi:[10.1006/ndsh.1995.1025](https://doi.org/10.1006/ndsh.1995.1025).

- [79] E. Browne, H. Junde, Nuclear Data Sheets for  $A=174$ , Nucl. Data Sheets 87 (1999) 15 – 176.  
doi:[10.1006/ndsh.1999.0015](https://doi.org/10.1006/ndsh.1999.0015).

## Figures

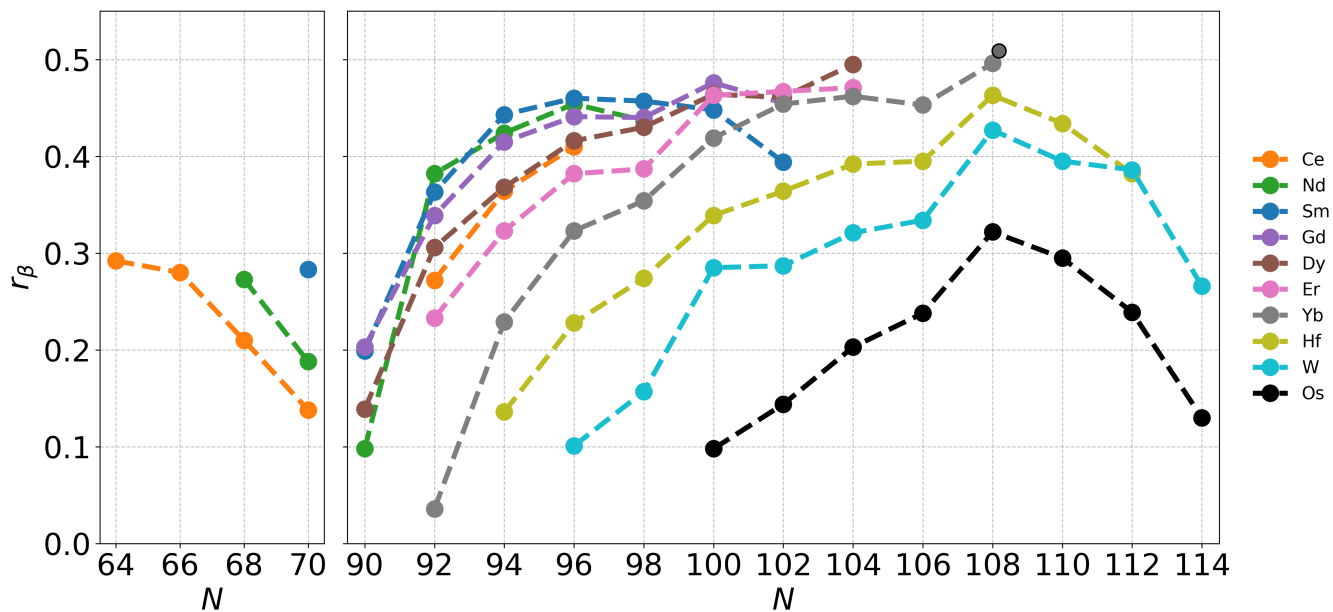


**Fig. 2:** Evolution of the CBS parameter  $r_\beta$  along the even-even isotopic chains of Ce-Os elements as a function of neutron number  $N$ . The bold gray point at  $^{178}\text{Yb}$  ( $N = 108$ ) represents the value  $r_\beta = 0.509$ , obtained from the CBS calculation, based on new measurements reported in [66].

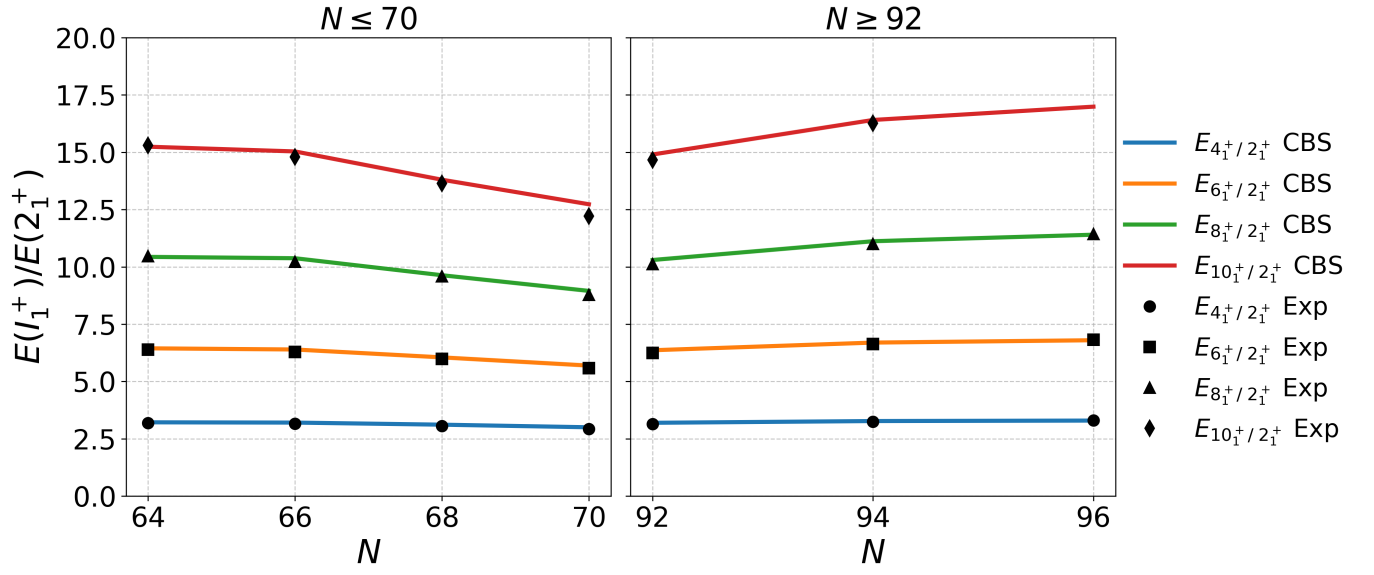


**Fig. 3:** Systematics of energy ratios  $E(I_1^+)/E(2_1^+)$  for the ground-state band of even-even Ce ( $Z=58$ ) isotopes as a function of neutron number  $N$ . Solid lines indicate CBS predictions, while experimental values are shown as symbols. Experimental uncertainties are smaller than the symbol sizes.

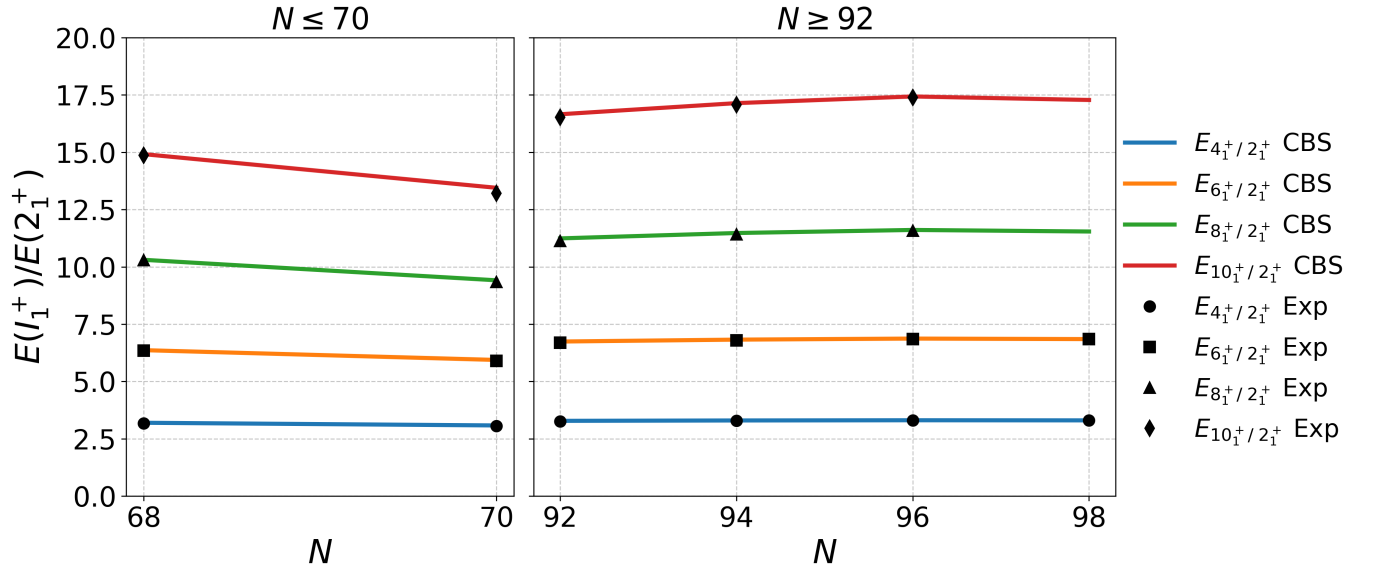


**Fig. 4:** Systematics of energy ratios  $E(I_1^+)/E(2_1^+)$  for the ground-state band of even-even Nd ( $Z=60$ ) isotopes as a function of neutron number  $N$ . Solid lines indicate CBS predictions, while experimental values are shown as symbols. Experimental uncertainties are smaller than the symbol sizes.

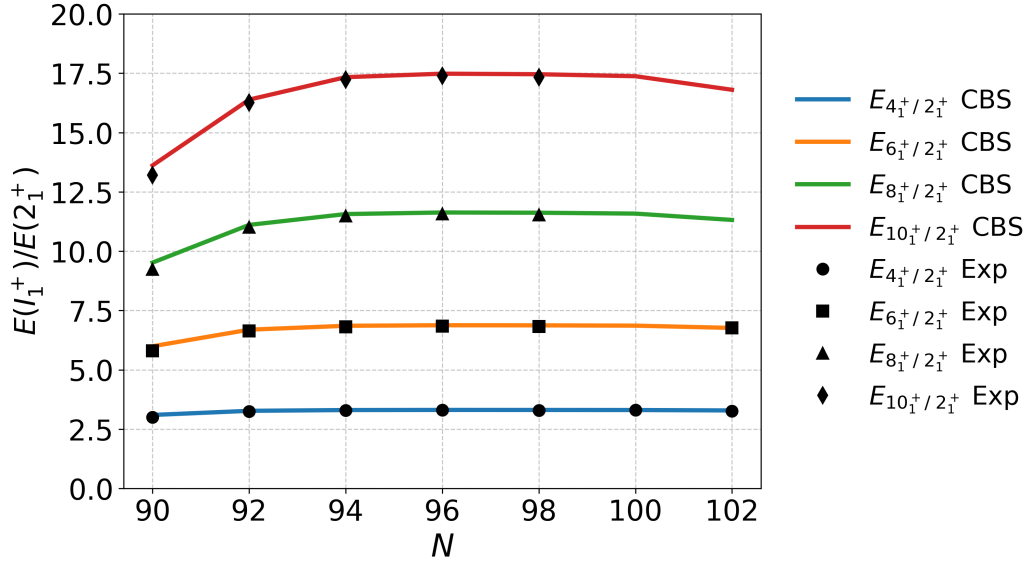


**Fig. 5:** Systematics of energy ratios  $E(I_1^+)/E(2_1^+)$  for the ground-state band of even-even Sm ( $Z=62$ ) isotopes as a function of neutron number  $N$ . Solid lines indicate CBS predictions, while experimental values are shown as symbols. Experimental uncertainties are smaller than the symbol sizes. The CBS results for  $^{132}\text{Sm}$  are omitted from the figure for clarity and can be found in Tables A, B, and C.

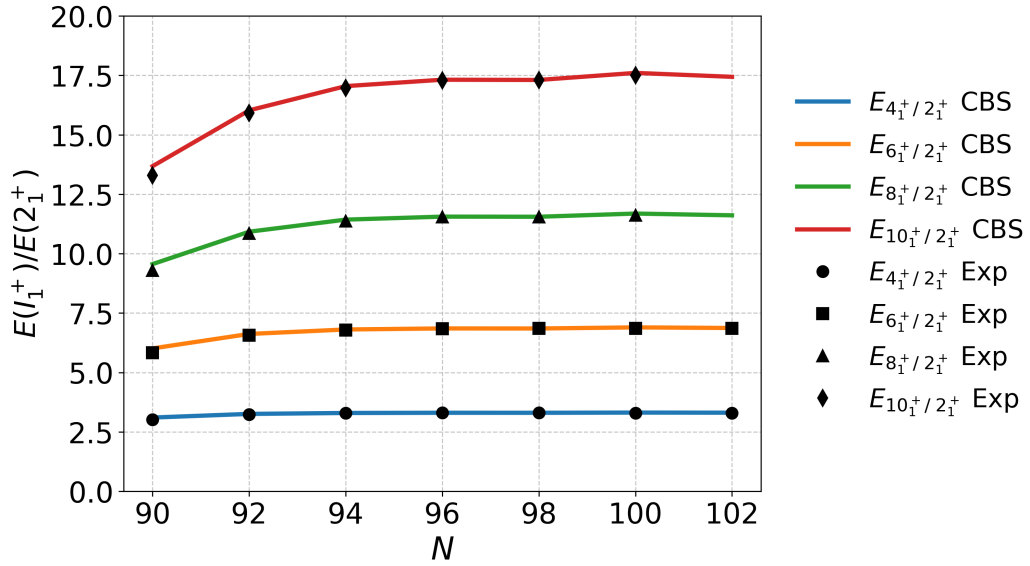


**Fig. 6:** Systematics of energy ratios  $E(I_1^+)/E(2_1^+)$  for the ground-state band of even-even Gd ( $Z=64$ ) isotopes as a function of neutron number  $N$ . Solid lines indicate CBS predictions, while experimental values are shown as symbols. Experimental uncertainties are smaller than the symbol sizes.

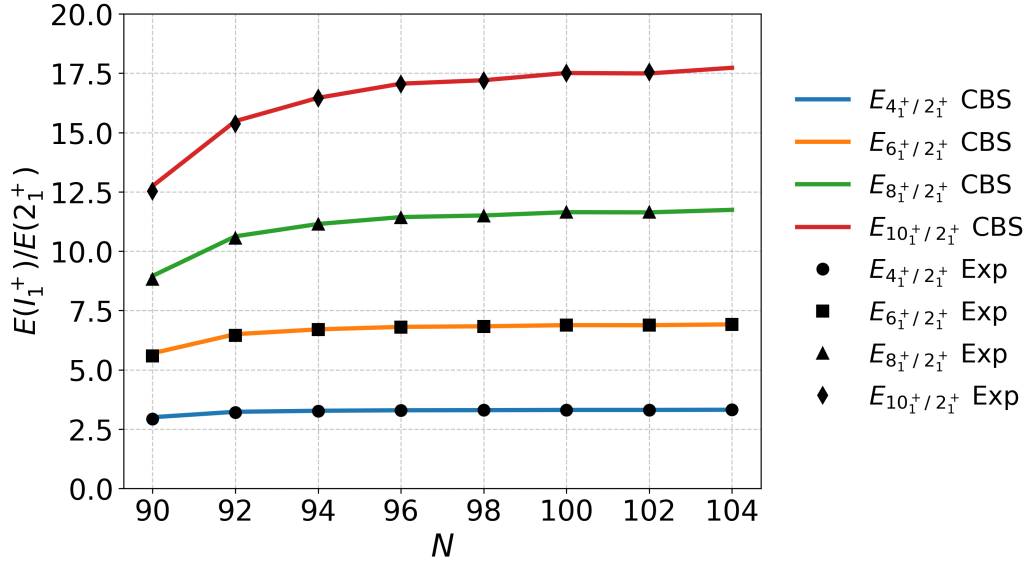


**Fig. 7:** Systematics of energy ratios  $E(I_1^+)/E(2_1^+)$  for the ground-state band of even-even Dy ( $Z=66$ ) isotopes as a function of neutron number  $N$ . Solid lines indicate CBS predictions, while experimental values are shown as symbols. Experimental uncertainties are smaller than the symbol sizes.

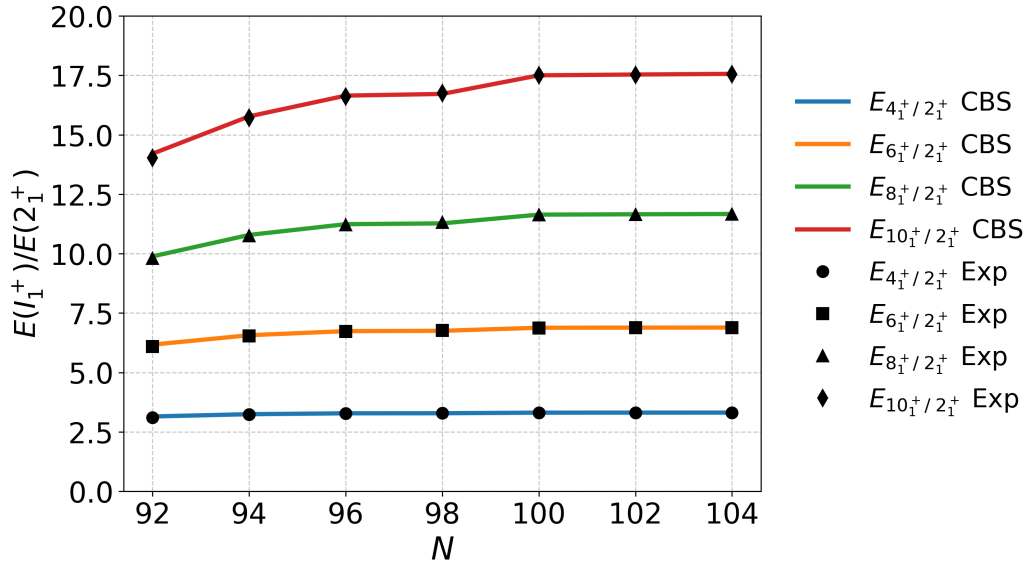


**Fig. 8:** Systematics of energy ratios  $E(I_1^+)/E(2_1^+)$  for the ground-state band of even-even Er ( $Z=68$ ) isotopes as a function of neutron number  $N$ . Solid lines indicate CBS predictions, while experimental values are shown as symbols. Experimental uncertainties are smaller than the symbol sizes.

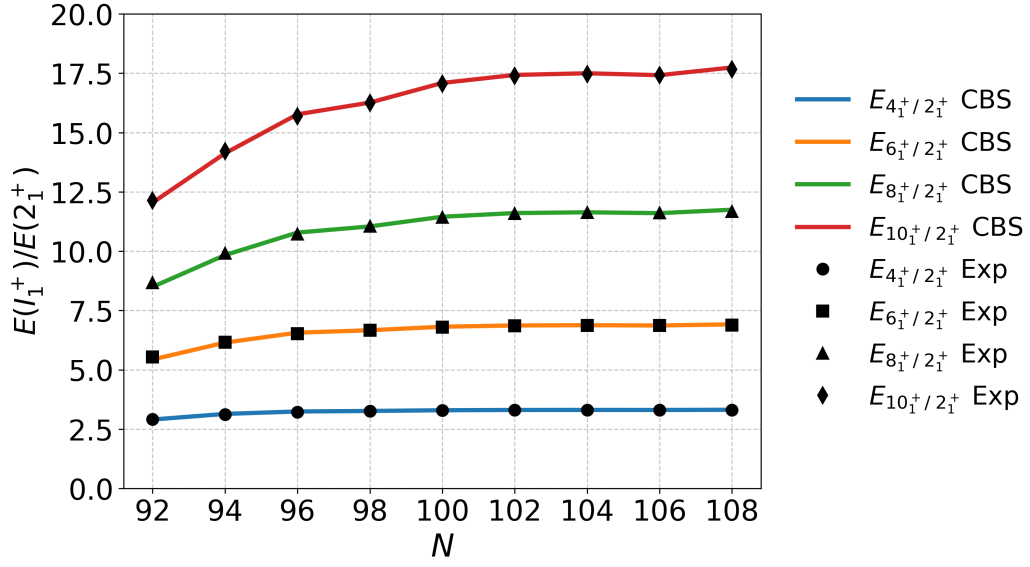


**Fig. 9:** Systematics of energy ratios  $E(I_1^+)/E(2_1^+)$  for the ground-state band of even-even Yb ( $Z=70$ ) isotopes as a function of neutron number  $N$ . Solid lines indicate CBS predictions, while experimental values are shown as symbols. Experimental uncertainties are smaller than the symbol sizes.

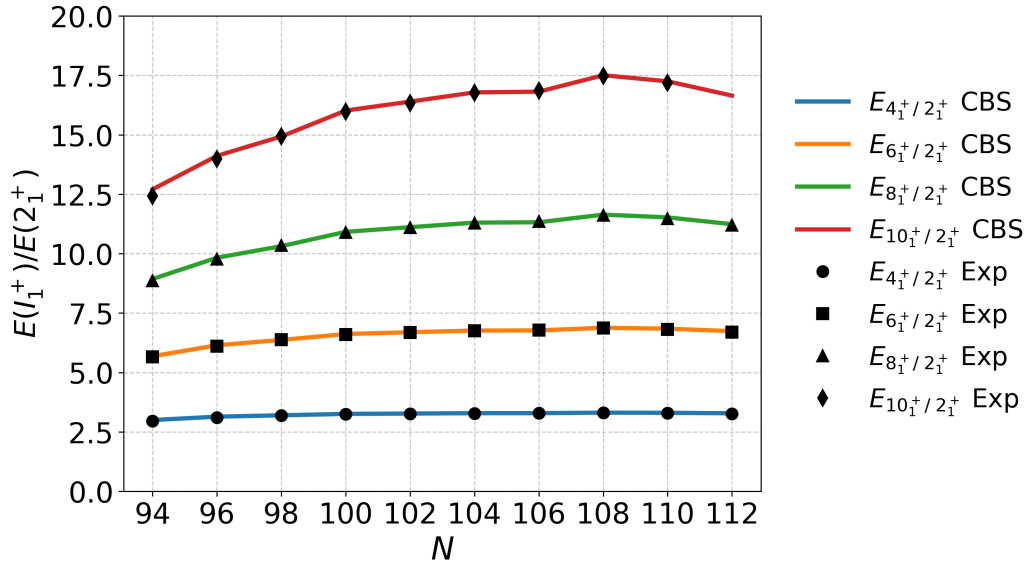


**Fig. 10:** Systematics of energy ratios  $E(I_1^+)/E(2_1^+)$  for the ground-state band of even-even Hf ( $Z=72$ ) isotopes as a function of neutron number  $N$ . Solid lines indicate CBS predictions, while experimental values are shown as symbols. Experimental uncertainties are smaller than the symbol sizes.

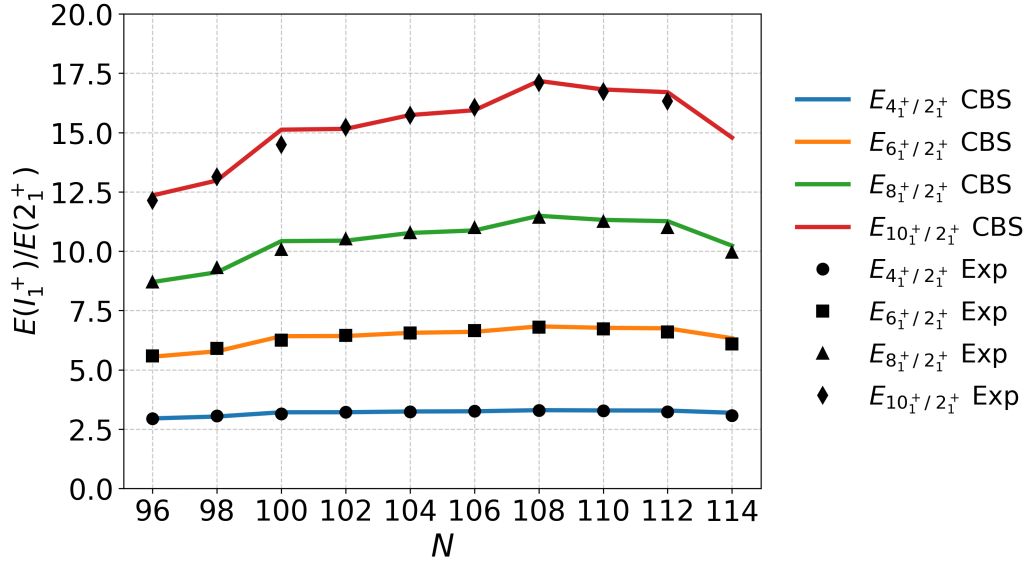


**Fig. 11:** Systematics of energy ratios  $E(I_1^+)/E(2_1^+)$  for the ground-state band of even-even W ( $Z=74$ ) isotopes as a function of neutron number  $N$ . Solid lines indicate CBS predictions, while experimental values are shown as symbols. Experimental uncertainties are smaller than the symbol sizes.

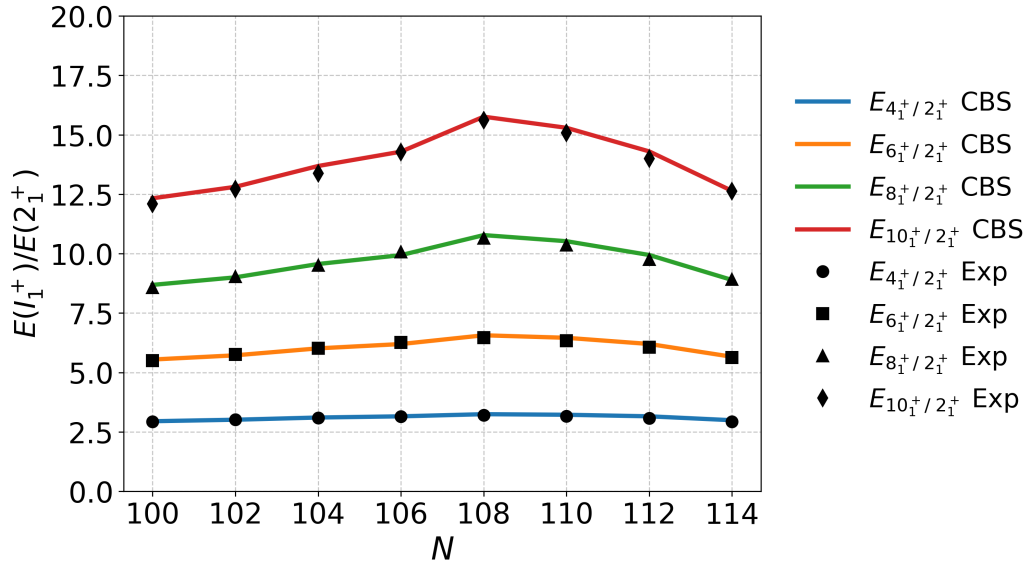


**Fig. 12:** Systematics of energy ratios  $E(I_1^+)/E(2_1^+)$  for the ground-state band of even-even Os ( $Z=76$ ) isotopes as a function of neutron number  $N$ . Solid lines indicate CBS predictions, while experimental values are shown as symbols. Experimental uncertainties are smaller than the symbol sizes.

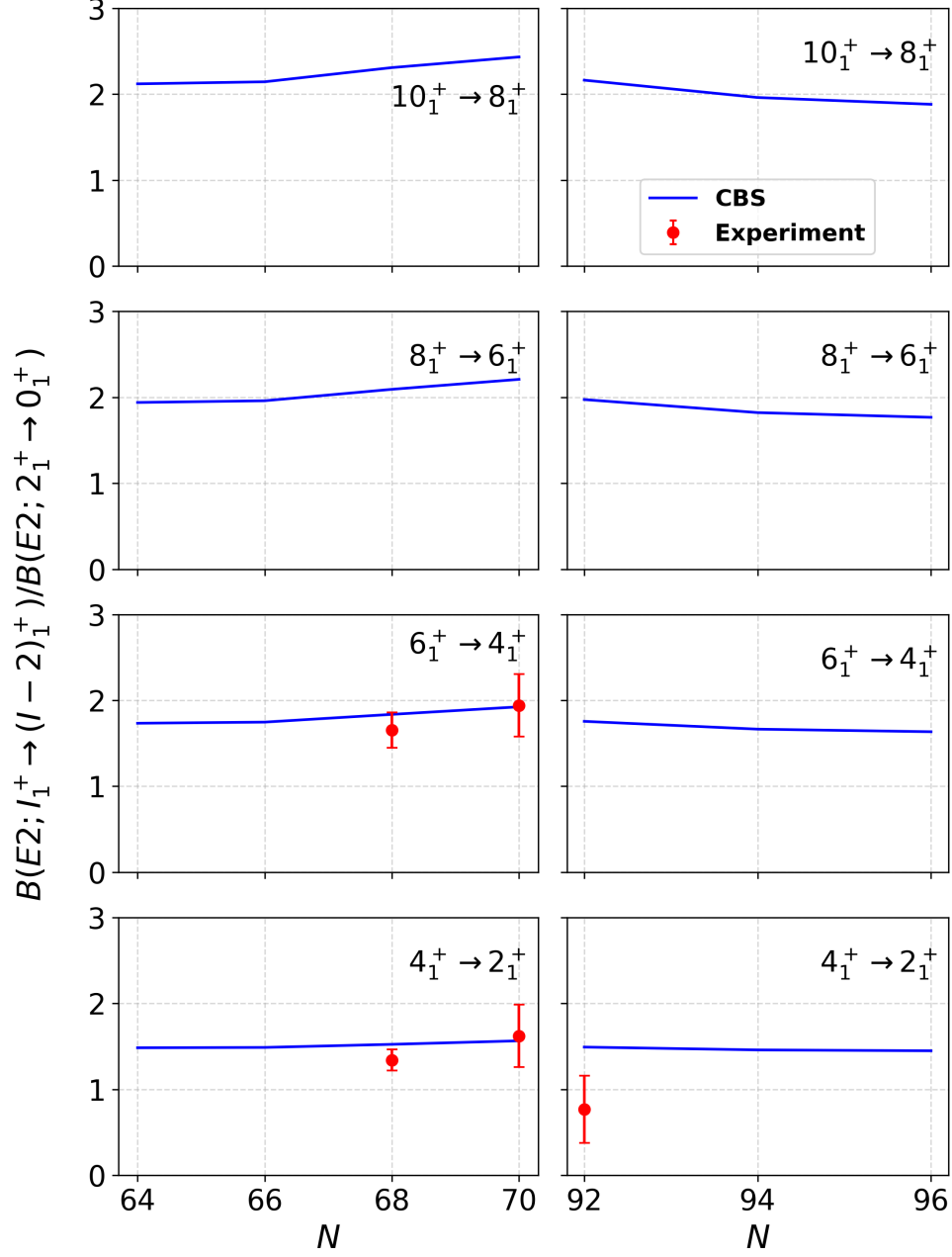


**Fig. 13:** Systematics of reduced electric quadrupole transition ratios  $B(E2; I_1^+ \rightarrow I_1^+ - 2) / B(E2; 2_1^+ \rightarrow 0_1^+)$  for the ground-state band of even-even Ce ( $Z=58$ ) isotopes as a function of neutron number  $N$ . Solid lines indicate CBS predictions, while experimental values are shown as symbols. Experimental data were retrieved from [24, 27, 28]. When multiple measurements were available, the most recent values were used.

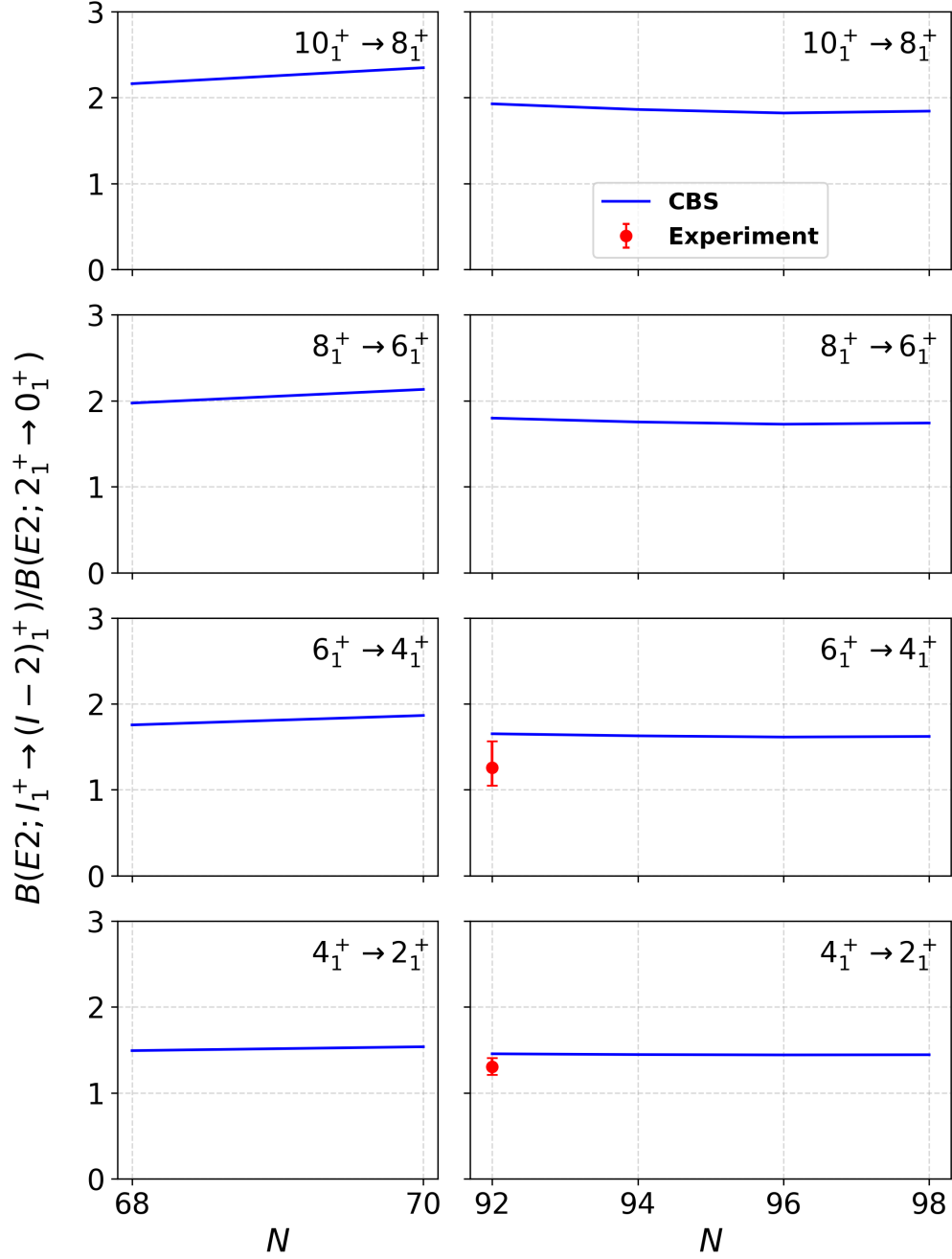


**Fig. 14:** Systematics of reduced electric quadrupole transition ratios  $B(E2; I_1^+ \rightarrow I_1^+ - 2) / B(E2; 2_1^+ \rightarrow 0_1^+)$  for the ground-state band of even-even Nd ( $Z=60$ ) isotopes as a function of neutron number  $N$ . Solid lines indicate CBS predictions, while experimental values are shown as symbols. Experimental data were retrieved from [25, 27]. When multiple measurements were available, the most recent values were used.

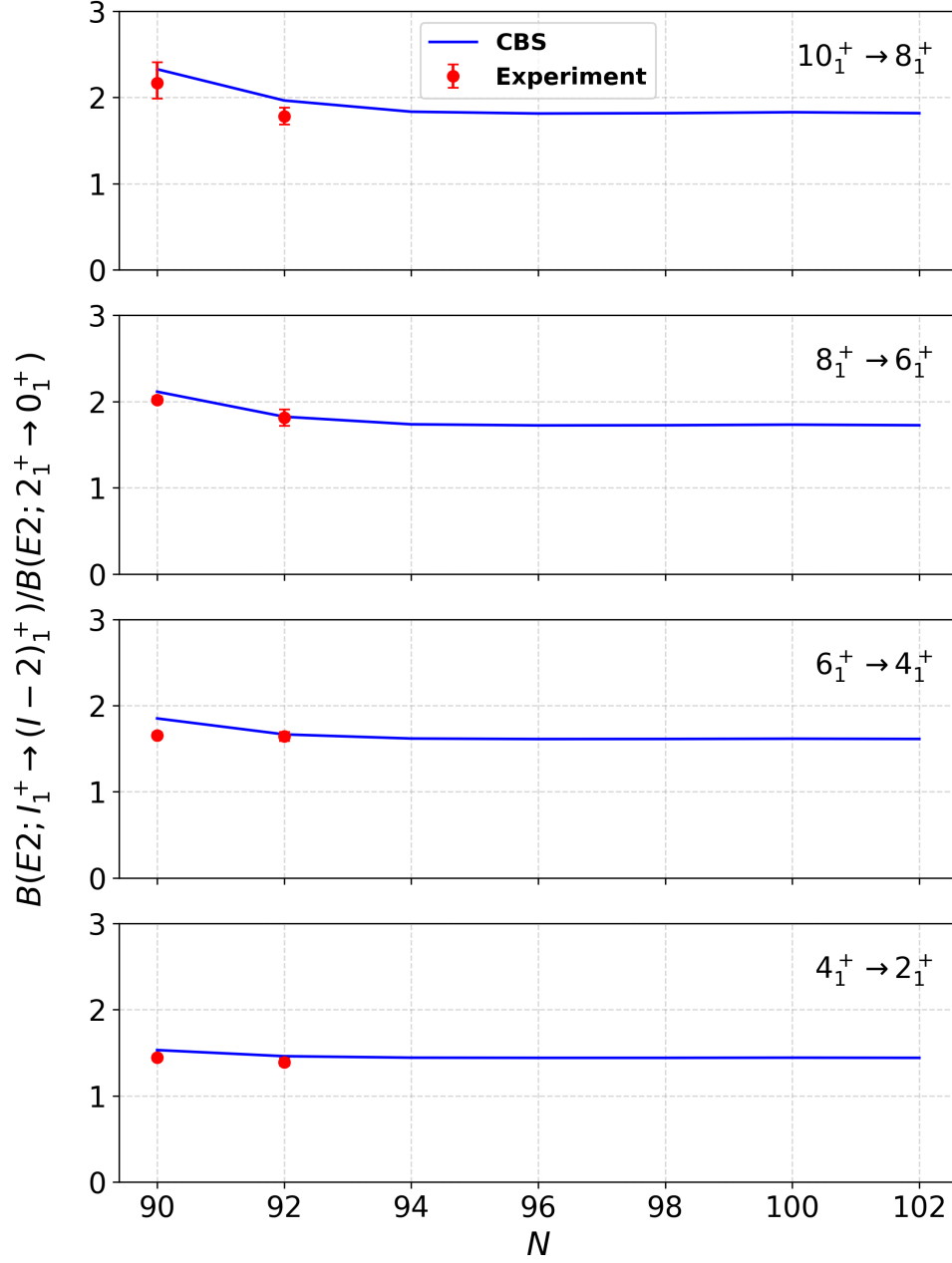


**Fig. 15:** Systematics of reduced electric quadrupole transition ratios  $B(E2; I_1^+ \rightarrow I_1^+ - 2) / B(E2; 2_1^+ \rightarrow 0_1^+)$  for the ground-state band of even-even Sm ( $Z=62$ ) isotopes as a function of neutron number  $N$ . Solid lines indicate CBS predictions, while experimental values are shown as symbols. Experimental data were retrieved from [25, 26]. When multiple measurements were available, the most recent values were used. The CBS results for  $^{132}\text{Sm}$  are omitted from the figure for clarity and can be found in Tables A, B, and C.

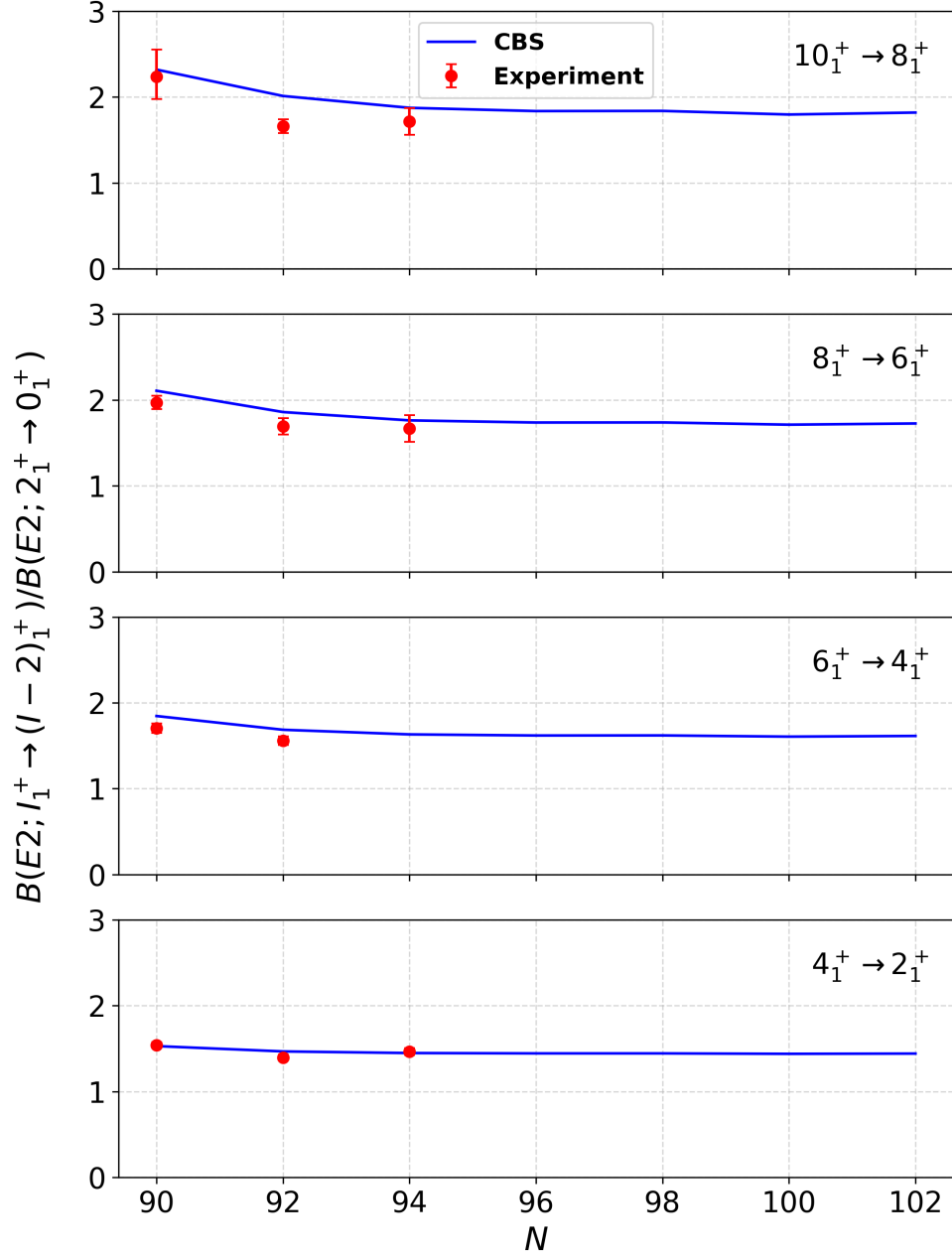


**Fig. 16:** Systematics of reduced electric quadrupole transition ratios  $B(E2; I_1^+ \rightarrow I_1^+ - 2) / B(E2; 2_1^+ \rightarrow 0_1^+)$  for the ground-state band of even-even Gd ( $Z=64$ ) isotopes as a function of neutron number  $N$ . Solid lines indicate CBS predictions, while experimental values are shown as symbols. Experimental data were retrieved from [26, 29, 30]. When multiple measurements were available, the most recent values were used.

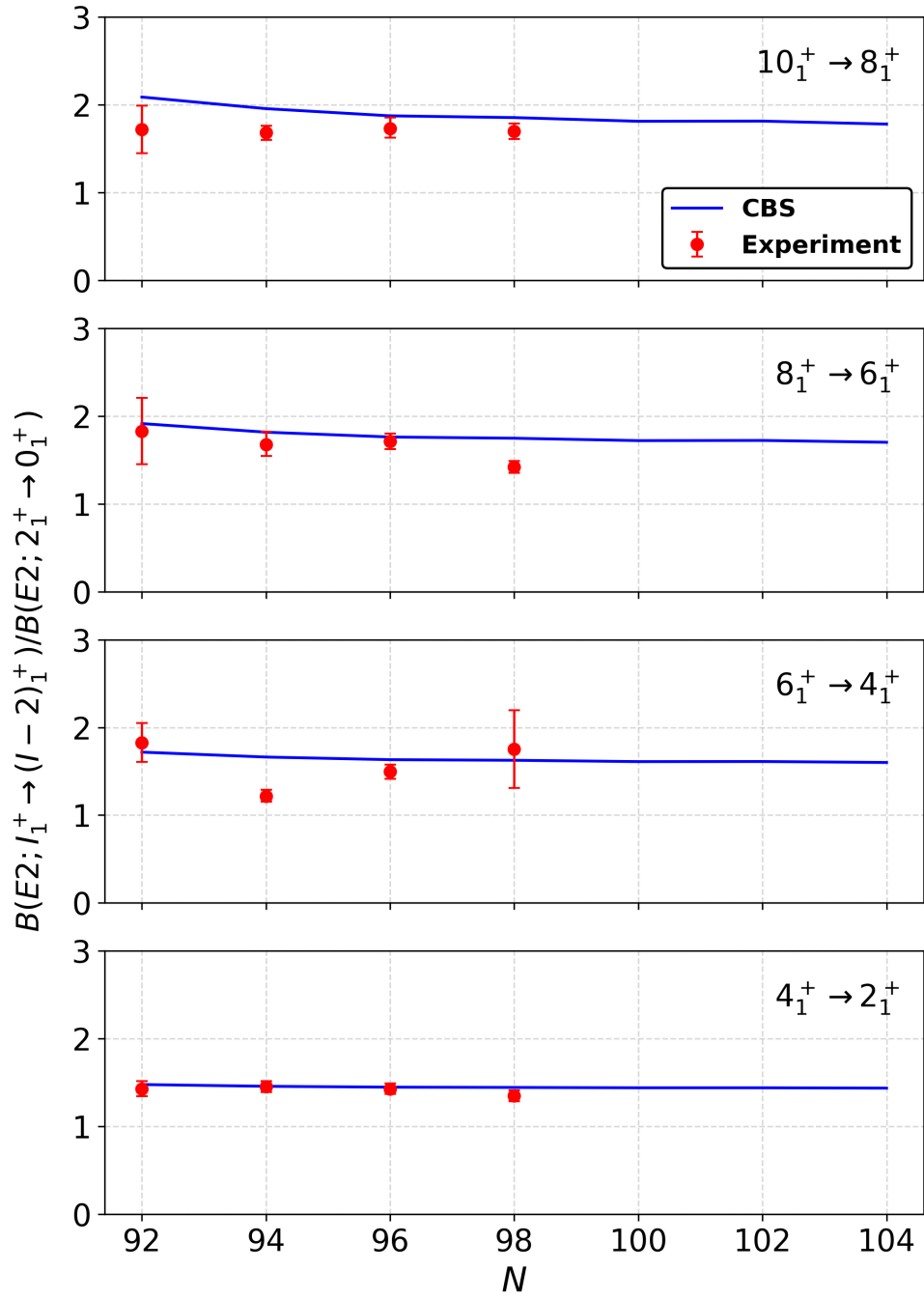


**Fig. 17:** Systematics of reduced electric quadrupole transition ratios  $B(E2; I_1^+ \rightarrow I_1^+ - 2) / B(E2; 2_1^+ \rightarrow 0_1^+)$  for the ground-state band of even-even Dy ( $Z=66$ ) isotopes as a function of neutron number  $N$ . Solid lines indicate CBS predictions, while experimental values are shown as symbols. Experimental data were retrieved from [29–32, 49, 77]. When multiple measurements were available, the most recent values were used.

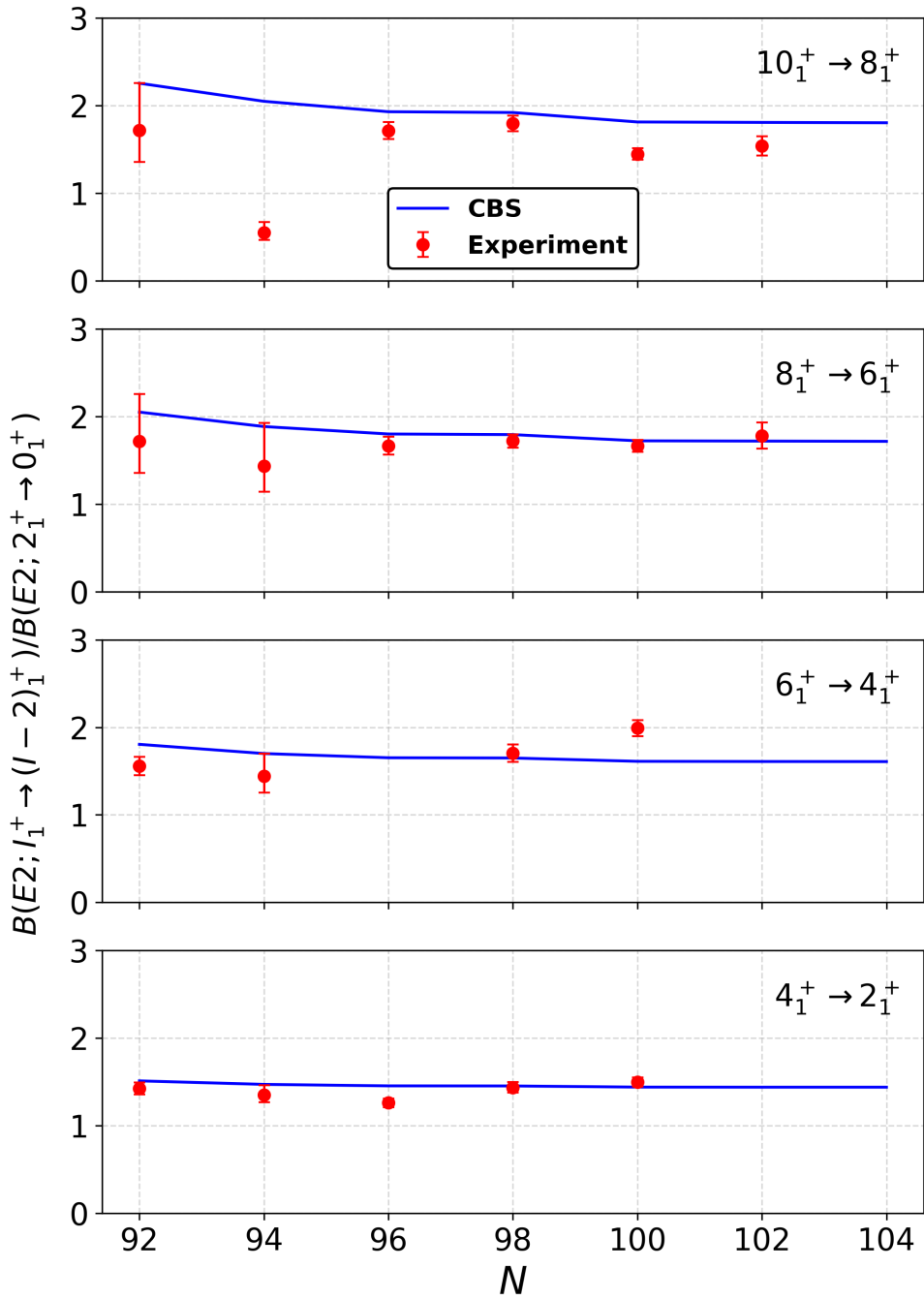


**Fig. 18:** Systematics of reduced electric quadrupole transition ratios  $B(E2; I_1^+ \rightarrow I_1^+ - 2) / B(E2; 2_1^+ \rightarrow 0_1^+)$  for the ground-state band of even-even Er ( $Z=68$ ) isotopes as a function of neutron number  $N$ . Solid lines indicate CBS predictions, while experimental values are shown as symbols. Experimental data were retrieved from [22, 31, 33–36]. When multiple measurements were available, the most recent values were used.

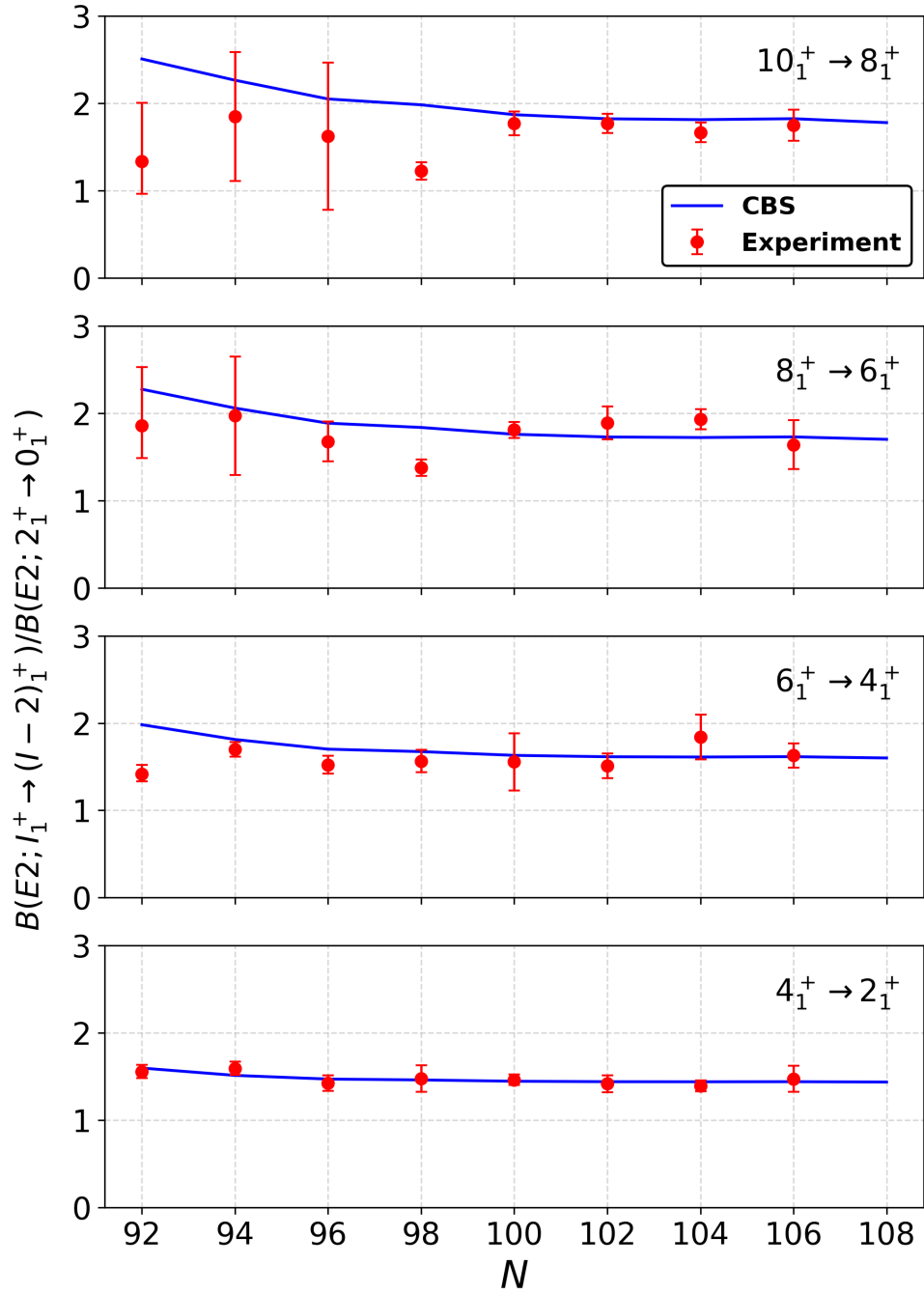


**Fig. 19:** Systematics of reduced electric quadrupole transition ratios  $B(E2; I_1^+ \rightarrow I_1^+ - 2) / B(E2; 2_1^+ \rightarrow 0_1^+)$  for the ground-state band of even-even Yb ( $Z=70$ ) isotopes as a function of neutron number  $N$ . Solid lines indicate CBS predictions, while experimental values are shown as symbols. Experimental data were retrieved from [32, 34, 36, 50, 51, 77]. When multiple measurements were available, the most recent values were used.

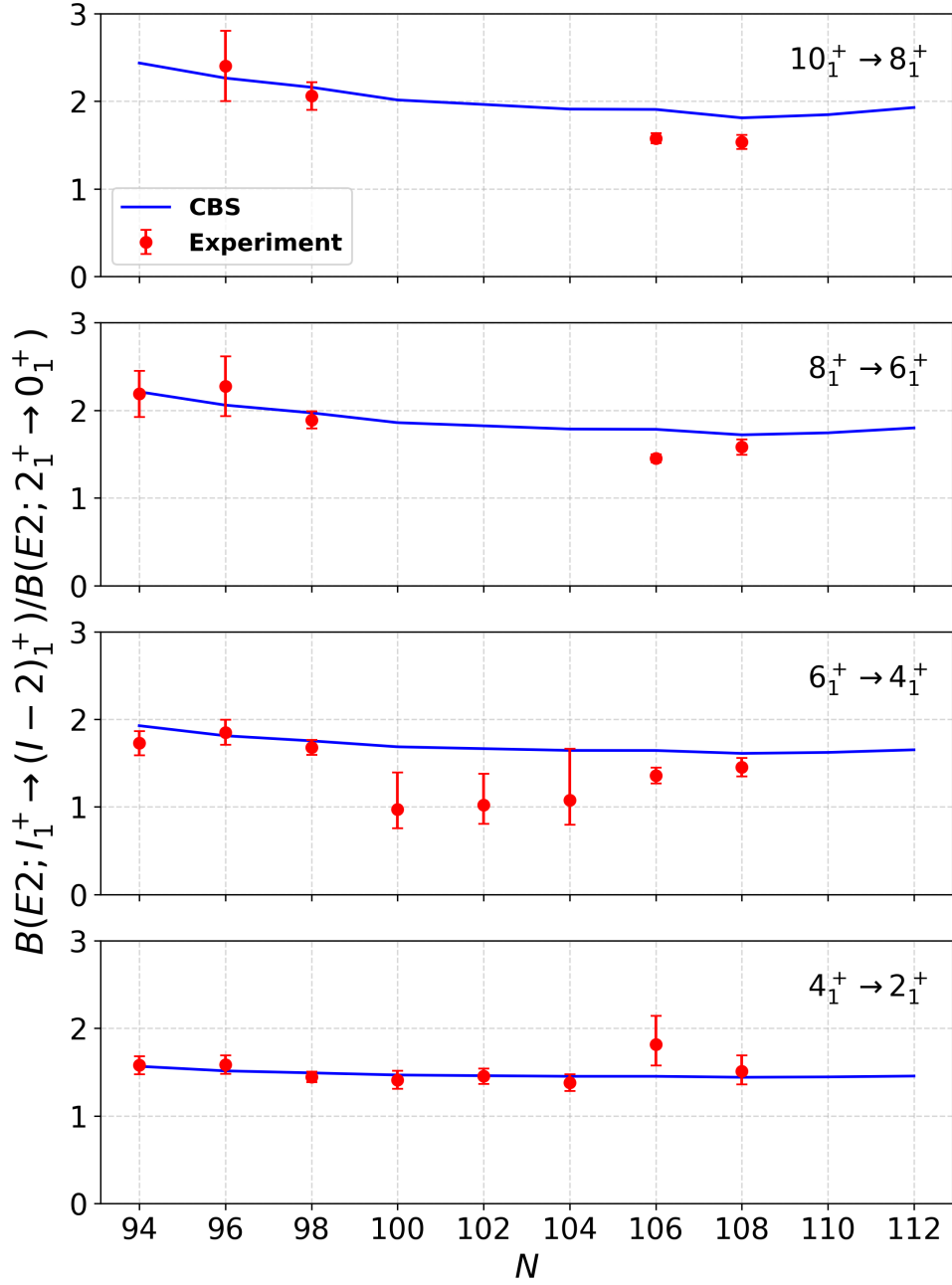


**Fig. 20:** Systematics of reduced electric quadrupole transition ratios  $B(E2; I_1^+ \rightarrow I_1^+ - 2) / B(E2; 2_1^+ \rightarrow 0_1^+)$  for the ground-state band of even-even Hf ( $Z=72$ ) isotopes as a function of neutron number  $N$ . Solid lines indicate CBS predictions, while experimental values are shown as symbols. Experimental data were retrieved from [34–36, 52, 53]. When multiple measurements were available, the most recent values were used.

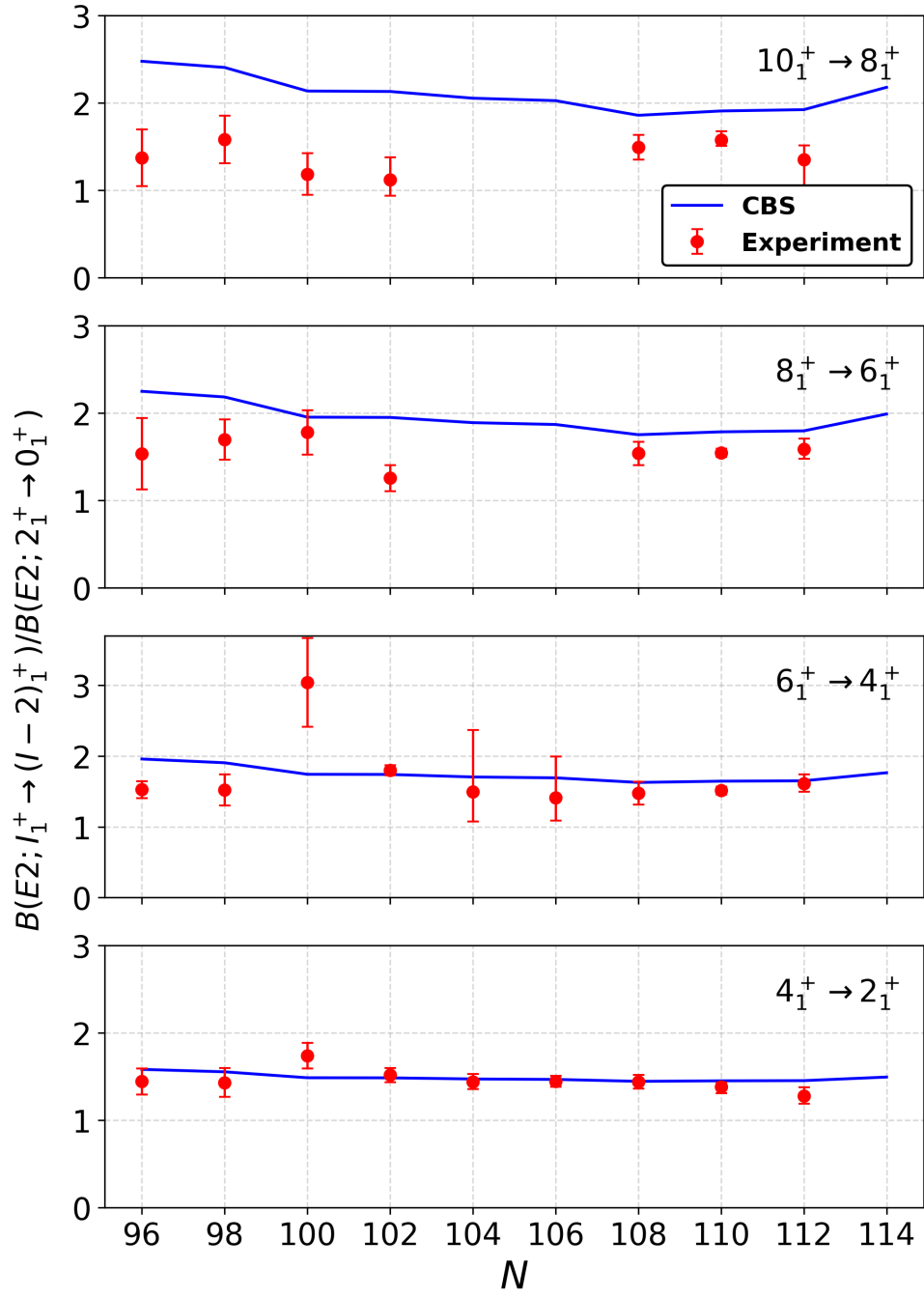


**Fig. 21:** Systematics of reduced electric quadrupole transition ratios  $B(E2; I_1^+ \rightarrow I_1^+ - 2) / B(E2; 2_1^+ \rightarrow 0_1^+)$  for the ground-state band of even-even W ( $Z=74$ ) isotopes as a function of neutron number  $N$ . Solid lines indicate CBS predictions, while experimental values are shown as symbols. Experimental data were retrieved from [36, 42–44, 54, 78, 79]. When multiple measurements were available, the most recent values were used.

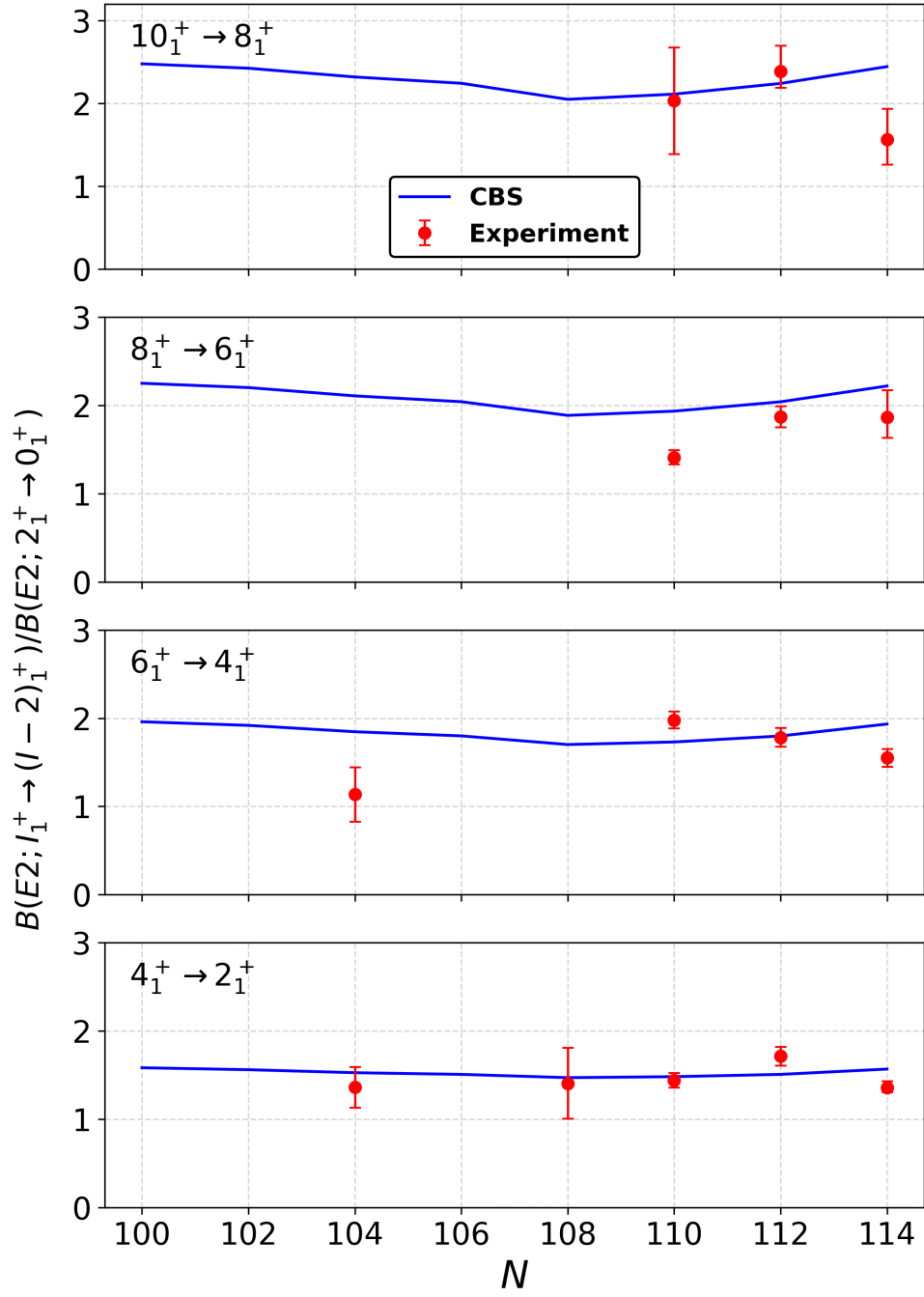


**Fig. 22:** Systematics of reduced electric quadrupole transition ratios  $B(E2; I_1^+ \rightarrow I_1^+ - 2) / B(E2; 2_1^+ \rightarrow 0_1^+)$  for the ground-state band of even-even Os ( $Z=76$ ) isotopes as a function of neutron number  $N$ . Solid lines indicate CBS predictions, while experimental values are shown as symbols. Experimental data were retrieved from [40, 43–46, 55]. When multiple measurements were available, the most recent values were used.

## Explanation of Tables

**Table A. Comparison between theoretical (CBS) and experimental energy ratios.**

Comparison between experimental (*Exp.*) data and theoretical predictions obtained within the Confined  $\beta$ -Soft (CBS) rotor model for even–even nuclei in the rare-earth region. The table presents ratios of excitation energies in the ground-state band,

$$E(I_1^+)/E(2_1^+),$$

where  $I_1^+$  denotes the spin of the excited state. For each observable, the CBS result is listed alongside the corresponding experimental value, where available. The parameter  $r_\beta$  denotes the confinement parameter of the CBS model and is determined independently for each nucleus.

Isotope	Even–even nucleus under consideration
$r_\beta$	CBS confinement parameter determined from the fit
$E(4_1^+)/E(2_1^+), E(6_1^+)/E(2_1^+), \dots$	Energy ratios for the ground-state band
CBS	Predictions obtained from the CBS model
Exp.	Experimental values taken from evaluated data (ENSDF)

**Table B. Comparison between theoretical (CBS) and experimental  $B(E2)$  transition ratios.**

Comparison between experimental (*Exp.*) data and theoretical predictions obtained within the Confined  $\beta$ -Soft (CBS) rotor model for even–even nuclei in the rare-earth region. The table presents reduced electric quadrupole transition-probability ratios in the ground-state band,

$$\frac{B(E2; I_1^+ \rightarrow (I_1 - 2)_1^+)}{B(E2; 2_1^+ \rightarrow 0_1^+)},$$

where  $I_1^+$  denotes the spin of the initial state ( $I \neq 2$ ). For each observable, the CBS result is listed alongside the corresponding experimental value, where available.

Isotope	Even–even nucleus under consideration
$r_\beta$	CBS confinement parameter determined from the fit
$B(E2; I_1^+ \rightarrow (I_1 - 2)_1^+)/B(E2; 2_1^+ \rightarrow 0_1^+)$	Reduced transition-probability ratios for the ground-state band
CBS	Predictions obtained from the CBS model
Exp.	Experimental values taken from evaluated data (ENSDF)

**Table C. CBS predictions for  $\beta$ -band excitation energies and  $B(E2)$  transition ratios.**

Predictions obtained within the Confined  $\beta$ -Soft (CBS) rotor model for even–even nuclei in the rare-earth region. The table presents excitation energies (in keV) of the  $\beta$ -band,

$$E(I_\beta^+), \quad I_\beta^+ = 0_\beta^+, 2_\beta^+, 4_\beta^+, 6_\beta^+,$$

where  $I_\beta^+$  denotes the spin/parity of states belonging to the  $\beta$ -band. For each nucleus, the CBS prediction is listed. The parameter  $r_\beta$  denotes the confinement parameter of the CBS model and is determined independently for each nucleus. In addition, the table includes CBS predictions for intraband reduced electric quadrupole transition ratios within the  $\beta$  band,

$$\frac{B(E2; 4_\beta^+ \rightarrow 2_\beta^+)}{B(E2; 2_\beta^+ \rightarrow 0_\beta^+)}, \quad \frac{B(E2; 6_\beta^+ \rightarrow 4_\beta^+)}{B(E2; 2_\beta^+ \rightarrow 0_\beta^+)}.$$

Isotope	Even–even nucleus under consideration
$r_\beta$	CBS confinement parameter determined from the fit
$E(I_\beta^+)$	CBS excitation energies (keV) of $\beta$ -band states
CBS	Predictions obtained from the CBS model
CBS $B(E2)$ ratios	Intraband $\beta$ -band transition ratios predicted by the CBS model

Table A: Energy ratios for even–even nuclei in the ground-state band. CBS results are compared with experimental values.

Isotope	$r_\beta$	Energy ratios							
		$\frac{E(4_1^+)}{E(2_1^+)}$		$\frac{E(6_1^+)}{E(2_1^+)}$		$\frac{E(8_1^+)}{E(2_1^+)}$		$\frac{E(10_1^+)}{E(2_1^+)}$	
		CBS	Exp	CBS	Exp	CBS	Exp	CBS	Exp
$^{122}\text{Ce}$	0.292	3.219	3.187	6.447	6.394	10.436	10.474	15.242	15.298
$^{124}\text{Ce}$	0.280	3.207	3.156	6.396	6.285	10.377	10.223	15.036	14.799
$^{126}\text{Ce}$	0.210	3.116	3.061	6.052	5.985	9.636	9.585	13.802	13.639
$^{128}\text{Ce}$	0.138	3.003	2.930	5.694	5.587	8.952	8.785	12.732	12.219
$^{150}\text{Ce}$	0.272	3.198	3.152	6.363	6.252	10.300	10.130	14.903	14.666
$^{152}\text{Ce}$	0.364	3.274	3.251	6.697	6.632	11.119	11.010	16.409	16.269
$^{154}\text{Ce}$	0.410	3.295	3.307	6.800	6.823	11.404	11.440	16.989	—
$^{128}\text{Nd}$	0.273	3.199	3.176	6.367	6.344	10.308	10.303	14.918	14.863
$^{130}\text{Nd}$	0.188	3.083	3.052	5.940	5.901	9.415	9.350	13.450	13.206
$^{150}\text{Nd}$	0.098	2.950	2.926	5.547	5.530	8.687	8.673	12.331	12.276
$^{152}\text{Nd}$	0.382	3.283	3.267	6.743	6.686	11.243	11.135	16.657	16.522
$^{154}\text{Nd}$	0.424	3.300	3.296	6.826	6.800	11.477	11.421	17.143	17.077
$^{156}\text{Nd}$	0.454	3.309	3.306	6.872	6.853	11.611	11.579	17.434	17.396
$^{158}\text{Nd}$	0.437	3.304	3.302	6.849	6.844	11.543	—	17.281	—
$^{132}\text{Sm}$	0.283	3.210	3.183	6.410	6.359	10.407	10.336	15.092	14.977
$^{152}\text{Sm}$	0.199	3.099	3.009	5.994	5.803	9.521	9.238	13.617	13.212
$^{154}\text{Sm}$	0.363	3.273	3.255	6.693	6.637	11.109	11.011	16.389	16.263
$^{156}\text{Sm}$	0.443	3.306	3.290	6.857	6.814	11.566	11.484	17.336	17.230
$^{158}\text{Sm}$	0.460	3.311	3.300	6.880	6.845	11.632	11.572	17.482	17.397
$^{160}\text{Sm}$	0.457	3.310	3.293	6.876	6.829	11.622	11.538	17.459	17.340
$^{162}\text{Sm}$	0.448	3.307	3.304	6.863	—	11.585	—	17.376	—
$^{164}\text{Sm}$	0.384	3.289	3.259	6.767	6.771	11.318	—	16.804	—
$^{154}\text{Gd}$	0.203	3.105	3.014	6.014	5.833	9.561	9.300	13.681	13.299
$^{156}\text{Gd}$	0.339	3.258	3.239	6.622	6.572	10.924	10.853	16.030	15.921
$^{158}\text{Gd}$	0.415	3.297	3.289	6.810	6.781	11.432	11.372	17.049	16.972
$^{160}\text{Gd}$	0.441	3.306	3.301	6.854	6.841	11.558	11.541	17.318	17.288
$^{162}\text{Gd}$	0.440	3.305	3.307	6.852	6.851	11.553	11.553	17.308	17.306
$^{164}\text{Gd}$	0.476	3.314	3.294	6.898	6.861	11.687	11.624	17.605	17.509
$^{166}\text{Gd}$	0.455	3.309	3.297	6.873	6.851	11.613	—	17.440	—
$^{156}\text{Dy}$	0.139	3.004	2.934	5.699	5.592	8.960	8.821	12.748	12.522
$^{158}\text{Dy}$	0.306	3.232	3.206	6.503	6.448	10.628	10.551	15.483	15.369
$^{160}\text{Dy}$	0.368	3.276	3.269	6.707	6.695	11.147	11.137	16.465	16.451

continued on next page

Table A – continued

Isotope	$r_\beta$	Energy ratios							
		$\frac{E(4_1^+)}{E(2_1^+)}$		$\frac{E(6_1^+)}{E(2_1^+)}$		$\frac{E(8_1^+)}{E(2_1^+)}$		$\frac{E(10_1^+)}{E(2_1^+)}$	
		CBS	Exp	CBS	Exp	CBS	Exp	CBS	Exp
$^{162}\text{Dy}$	0.416	3.297	3.294	6.812	6.803	11.438	11.422	17.061	17.049
$^{164}\text{Dy}$	0.430	3.302	3.300	6.836	6.831	11.507	11.492	17.207	17.183
$^{166}\text{Dy}$	0.464	3.311	3.311	6.884	6.883	11.645	11.646	17.511	17.511
$^{168}\text{Dy}$	0.461	3.311	3.313	6.881	6.884	11.637	11.651	17.492	17.546
$^{170}\text{Dy}$	0.495	3.318	3.321	6.917	6.920	11.743	—	17.731	—
$^{160}\text{Er}$	0.233	3.150	3.103	6.173	6.098	9.886	9.796	14.207	14.032
$^{162}\text{Er}$	0.323	3.246	3.231	6.568	6.534	10.788	10.751	15.776	15.710
$^{164}\text{Er}$	0.382	3.283	3.277	6.741	6.722	11.240	11.209	16.650	16.613
$^{166}\text{Er}$	0.387	3.286	3.289	6.754	6.772	11.274	11.312	16.720	16.756
$^{168}\text{Er}$	0.463	3.311	3.308	6.883	6.875	11.642	11.633	17.503	17.499
$^{170}\text{Er}$	0.467	3.312	3.310	6.888	6.880	11.657	11.644	17.537	17.520
$^{172}\text{Er}$	0.471	3.313	3.314	6.892	6.886	11.669	11.662	17.565	17.556
$^{162}\text{Yb}$	0.036	2.907	2.923	5.437	5.543	8.497	8.670	12.047	12.141
$^{164}\text{Yb}$	0.229	3.143	3.126	6.150	6.163	9.837	9.916	14.127	14.222
$^{166}\text{Yb}$	0.323	3.246	3.227	6.567	6.525	10.785	10.728	15.770	15.687
$^{168}\text{Yb}$	0.354	3.268	3.266	6.669	6.671	11.045	11.057	16.264	16.255
$^{170}\text{Yb}$	0.419	3.298	3.293	6.818	6.805	11.453	11.435	17.092	17.061
$^{172}\text{Yb}$	0.454	3.309	3.305	6.871	6.857	11.608	11.585	17.429	17.396
$^{174}\text{Yb}$	0.462	3.311	3.309	6.882	6.877	11.640	11.636	17.499	17.467
$^{176}\text{Yb}$	0.453	3.309	3.310	6.870	6.873	11.604	11.613	17.419	17.424
$^{178}\text{Yb}$	0.496	3.317	3.310	6.917	6.882	11.749	11.682	17.744	17.661
$^{166}\text{Hf}$	0.136	3.000	2.966	5.685	5.655	8.936	8.864	12.707	12.431
$^{168}\text{Hf}$	0.228	3.142	3.109	6.146	6.100	9.830	9.778	14.116	13.989
$^{170}\text{Hf}$	0.274	3.200	3.194	6.370	6.380	10.316	10.353	14.931	14.931
$^{172}\text{Hf}$	0.339	3.258	3.248	6.620	6.598	10.919	10.895	16.021	15.974
$^{174}\text{Hf}$	0.364	3.273	3.268	6.695	6.688	11.114	11.097	16.398	16.337
$^{176}\text{Hf}$	0.392	3.288	3.284	6.765	6.755	11.306	11.293	16.785	16.765
$^{178}\text{Hf}$	0.395	3.289	3.291	6.771	6.785	11.321	11.356	16.816	16.850
$^{180}\text{Hf}$	0.463	3.311	3.306	6.883	6.868	11.643	11.617	17.507	17.480
$^{182}\text{Hf}$	0.434	3.304	3.294	6.843	6.814	11.527	11.473	17.252	17.184
$^{184}\text{Hf}$	0.382	3.283	3.264	6.741	6.696	11.240	11.198	16.650	—
$^{170}\text{W}$	0.101	2.953	2.950	5.555	5.587	8.701	8.700	12.351	12.133

continued on next page

Table A – continued

Isotope	$r_\beta$	Energy ratios							
		$\frac{E(4_1^+)}{E(2_1^+)}$		$\frac{E(6_1^+)}{E(2_1^+)}$		$\frac{E(8_1^+)}{E(2_1^+)}$		$\frac{E(10_1^+)}{E(2_1^+)}$	
		CBS	Exp	CBS	Exp	CBS	Exp	CBS	Exp
$^{172}\text{W}$	0.157	3.033	3.061	5.782	5.906	9.114	9.308	12.981	13.127
$^{174}\text{W}$	0.285	3.212	3.154	6.418	6.247	10.426	10.079	15.122	14.491
$^{176}\text{W}$	0.287	3.214	3.215	6.426	6.458	10.445	10.524	15.157	15.222
$^{178}\text{W}$	0.321	3.245	3.236	6.561	6.555	10.769	10.779	15.739	15.726
$^{180}\text{W}$	0.334	3.254	3.260	6.604	6.648	10.877	10.993	15.942	16.070
$^{182}\text{W}$	0.427	3.301	3.289	6.832	6.796	11.493	11.427	17.177	17.095
$^{184}\text{W}$	0.395	3.289	3.273	6.771	6.728	11.321	11.260	16.817	16.734
$^{186}\text{W}$	0.386	3.285	3.234	6.751	6.600	11.266	11.003	16.703	16.329
$^{188}\text{W}$	0.266	3.191	3.071	6.333	6.085	10.233	9.957	14.789	—
$^{176}\text{Os}$	0.098	2.950	2.927	5.546	5.495	8.686	8.569	12.330	12.095
$^{178}\text{Os}$	0.144	3.013	3.016	5.723	5.761	9.004	9.031	12.812	12.721
$^{180}\text{Os}$	0.203	3.106	3.093	6.016	6.018	9.565	9.514	13.688	13.375
$^{182}\text{Os}$	0.238	3.156	3.154	6.197	6.258	9.937	10.073	14.291	14.276
$^{184}\text{Os}$	0.322	3.246	3.203	6.566	6.465	10.781	10.646	15.763	15.621
$^{186}\text{Os}$	0.295	3.222	3.166	6.460	6.335	10.524	10.361	15.296	15.082
$^{188}\text{Os}$	0.239	3.157	3.082	6.200	6.065	9.944	9.753	14.302	13.999
$^{190}\text{Os}$	0.130	2.992	2.934	5.662	5.624	8.893	8.924	12.642	12.624

Table B: Reduced transition-probability ratios for even–even nuclei in the ground-state band. CBS results are compared with experimental values.

Isotope	$r_\beta$	Transition ratios							
		$\frac{B(E2; 4_1^+ \rightarrow 2_1^+)}{B(E2; 2_1^+ \rightarrow 0_1^+)}$		$\frac{B(E2; 6_1^+ \rightarrow 4_1^+)}{B(E2; 2_1^+ \rightarrow 0_1^+)}$		$\frac{B(E2; 8_1^+ \rightarrow 6_1^+)}{B(E2; 2_1^+ \rightarrow 0_1^+)}$		$\frac{B(E2; 10_1^+ \rightarrow 8_1^+)}{B(E2; 2_1^+ \rightarrow 0_1^+)}$	
		CBS	Exp	CBS	Exp	CBS	Exp	CBS	Exp
$^{122}\text{Ce}$	0.292	1.484	—	1.734	—	1.940	—	2.121	—
$^{124}\text{Ce}$	0.280	1.488	—	1.747	—	1.960	—	2.145	—
$^{126}\text{Ce}$ [27]	0.210	1.524	1.341(264)	1.837	0.580(240)	2.093	0.652(119)	2.310	—
$^{128}\text{Ce}$ [28]	0.138	1.565	1.623(401)	1.925	1.712(487)	2.209	2.252(435)	2.434	2.342(597)
$^{150}\text{Ce}$ [24]	0.272	1.492	0.769(390)	1.756	—	1.974	—	2.164	—
$^{152}\text{Ce}$	0.364	1.459	—	1.665	—	1.822	—	1.962	—
$^{154}\text{Ce}$	0.410	1.449	—	1.635	—	1.767	—	1.883	—
$^{128}\text{Nd}$	0.273	1.492	—	1.755	—	1.973	—	2.162	—
$^{130}\text{Nd}$	0.188	1.537	—	1.865	—	2.132	—	2.348	—
$^{150}\text{Nd}$ [24]	0.098	1.584	1.558(43)	1.959	1.776(90)	2.248	1.862(204)	2.478	1.733(105)
$^{152}\text{Nd}$ [25]	0.382	1.455	1.306(99)	1.652	1.260( $^{+0.304}_{-0.215}$ )	1.798	—	1.928	—
$^{154}\text{Nd}$	0.424	1.446	—	1.628	—	1.753	—	1.862	—
$^{156}\text{Nd}$	0.454	1.442	—	1.614	—	1.727	—	1.821	—
$^{158}\text{Nd}$	0.437	1.444	—	1.621	—	1.741	—	1.843	—
$^{132}\text{Sm}$	0.283	1.487	—	1.743	—	1.954	—	2.139	—
$^{152}\text{Sm}$ [25]	0.199	1.531	1.445(22)	1.851	1.655(33)	2.114	2.021(35)	2.328	2.166( $^{+0.243}_{-0.181}$ )
$^{154}\text{Sm}$ [26]	0.363	1.460	1.392(42)	1.666	1.642(53)	1.824	1.813(96)	1.965	1.784(96)
$^{156}\text{Sm}$	0.443	1.443	—	1.618	—	1.736	—	1.835	—
$^{158}\text{Sm}$	0.460	1.441	—	1.612	—	1.723	—	1.814	—
$^{160}\text{Sm}$	0.457	1.441	—	1.613	—	1.725	—	1.818	—
$^{162}\text{Sm}$	0.448	1.443	—	1.616	—	1.732	—	1.829	—
$^{164}\text{Sm}$	0.457	1.441	—	1.613	—	1.725	—	1.818	—
$^{154}\text{Gd}$ [26]	0.203	1.529	1.542(31)	1.846	1.704(53)	2.107	1.970(78)	2.320	2.236( $^{+0.317}_{-0.260}$ )
$^{156}\text{Gd}$ [29]	0.339	1.467	1.397(31)	1.686	1.561(50)	1.859	1.693(94)	2.013	1.661(79)
$^{158}\text{Gd}$ [30]	0.415	1.448	1.465(42)	1.632	—	1.762	1.667(157)	1.875	1.717(157)
$^{160}\text{Gd}$	0.441	1.444	—	1.619	—	1.737	—	1.837	—
$^{162}\text{Gd}$	0.440	1.444	—	1.620	—	1.738	—	1.839	—
$^{164}\text{Gd}$	0.476	1.439	—	1.606	—	1.712	—	1.797	—
$^{166}\text{Gd}$	0.455	1.442	—	1.614	—	1.726	—	1.820	—
$^{156}\text{Dy}$ [29]	0.139	1.564	1.632(24)	1.923	1.760(89)	2.206	1.873(57)	2.432	2.067(201)
$^{158}\text{Dy}$ [30]	0.306	1.478	1.430(86)	1.718	1.828(219)	1.914	1.828(378)	2.087	1.720(271)
$^{160}\text{Dy}$ [31]	0.368	1.458	1.455(60)	1.662	1.216( $^{+0.073}_{-0.063}$ )	1.816	1.675( $^{+0.145}_{-0.129}$ )	1.955	1.680(80)

continued on next page

Table B – continued

Isotope	$r_\beta$	Transition ratios							
		$\frac{B(E2; 4_1^+ \rightarrow 2_1^+)}{B(E2; 2_1^+ \rightarrow 0_1^+)}$		$\frac{B(E2; 6_1^+ \rightarrow 4_1^+)}{B(E2; 2_1^+ \rightarrow 0_1^+)}$		$\frac{B(E2; 8_1^+ \rightarrow 6_1^+)}{B(E2; 2_1^+ \rightarrow 0_1^+)}$		$\frac{B(E2; 10_1^+ \rightarrow 8_1^+)}{B(E2; 2_1^+ \rightarrow 0_1^+)}$	
		CBS	Exp	CBS	Exp	CBS	Exp	CBS	Exp
$^{162}\text{Dy}$ [32]	0.416	1.448	1.430(59)	1.632	1.495(82)	1.761	1.712(88)	1.873	1.732( $^{+0.122}$ <sub>-0.107</sub> )
$^{164}\text{Dy}$	0.430	1.445	1.351(64) [49]	1.625	1.754(441) [49]	1.747	1.422(67) [77]	1.853	1.697(89)[77]
$^{166}\text{Dy}$ [49]	0.464	1.441	—	1.610	—	1.720	—	1.811	—
$^{168}\text{Dy}$	0.461	1.441	—	1.611	—	1.722	—	1.813	—
$^{170}\text{Dy}$	0.495	1.437	—	1.600	—	1.701	—	1.779	—
$^{160}\text{Er}$ [31]	0.233	1.512	1.426(69)	1.805	1.556(105)	2.049	1.716( $^{+0.536}$ <sub>-0.360</sub> )	2.254	1.716( $^{+0.536}$ <sub>-0.360</sub> )
$^{162}\text{Er}$ [22]	0.323	1.472	1.351( $^{+0.110}$ <sub>-0.084</sub> )	1.700	1.443( $^{+0.255}$ <sub>-0.191</sub> )	1.884	1.432( $^{+0.492}$ <sub>-0.293</sub> )	2.048	0.551( $^{+0.119}$ <sub>-0.087</sub> )
$^{164}\text{Er}$ [33]	0.382	1.455	1.262(149)	1.652	—	1.799	1.665(101)	1.929	1.714(97)
$^{166}\text{Er}$ [34]	0.387	1.454	1.438(61)	1.649	1.705(100)	1.792	1.719(76)	1.920	1.797(89)
$^{168}\text{Er}$ [35]	0.463	1.441	1.498(51)	1.611	1.991(92)	1.721	1.662(69)	1.812	1.446(67)
$^{170}\text{Er}$ [36]	0.467	1.440	—	1.609	—	1.718	1.779(148)	1.807	1.538(110)
$^{172}\text{Er}$	0.471	1.440	—	1.608	—	1.715	—	1.803	—
$^{162}\text{Yb}$ [32]	0.036	1.598	1.559(75)	1.981	1.418( $^{+0.102}$ <sub>-0.088</sub> )	2.274	1.856( $^{+0.669}$ <sub>-0.373</sub> )	2.507	1.336( $^{+0.669}$ <sub>-0.372</sub> )
$^{164}\text{Yb}$ [77]	0.229	1.514	1.595(76)	1.812	1.700(83)	2.058	1.970(680)	2.264	1.847(740)
$^{166}\text{Yb}$ [34]	0.323	1.472	1.424(88)	1.701	1.524(102)	1.885	1.675(227)	2.049	1.623(842)
$^{168}\text{Yb}$ [50]	0.354	1.462	1.478(151)	1.673	1.565(129)	1.836	1.373(94)	1.982	1.225(100)
$^{170}\text{Yb}$	0.419	1.447	1.463(61) [51]	1.630	1.556(328) [51]	1.758	1.800(159) [36]	1.869	1.771(135) [36]
$^{172}\text{Yb}$ [37]	0.454	1.442	1.420(95)	1.614	1.509(142)	1.727	1.887(190)	1.822	1.769(110)
$^{174}\text{Yb}$ [79]	0.462	1.441	1.393(62)	1.611	1.841(255)	1.721	1.930(116)	1.812	1.667(114)
$^{176}\text{Yb}$ [38]	0.453	1.442	1.475(148)	1.615	1.628(135)	1.728	1.639(280)	1.823	1.749(177)
$^{178}\text{Yb}$	0.496	1.438	—	1.600	—	1.701	—	1.778	—
$^{166}\text{Hf}$ [34]	0.136	1.566	1.578(102)	1.927	1.727(139)	2.211	2.188(263)	2.437	—
$^{168}\text{Hf}$ [35]	0.228	1.514	1.584(106)	1.812	1.851(144)	2.059	2.273(341)	2.265	2.403(405)
$^{170}\text{Hf}$ [36]	0.274	1.491	1.445(60)	1.754	1.681(85)	1.971	1.890(98)	2.160	2.060(158)
$^{172}\text{Hf}$	0.339	1.467	1.412(103) [52]	1.686	0.912( $^{+0.418}$ <sub>-0.218</sub> ) [52]	1.859	—	2.015	—
$^{174}\text{Hf}$	0.364	1.459	1.454(88) [53]	1.665	1.021( $^{+0.356}$ <sub>-0.212</sub> ) [53]	1.823	—	1.964	—
$^{176}\text{Hf}$	0.392	1.452	1.381(96) [53]	1.645	1.077( $^{+0.586}$ <sub>-0.282</sub> ) [52, 53]	1.786	—	1.911	—
$^{178}\text{Hf}$	0.395	1.452	1.816( $^{+0.327}$ <sub>-0.239</sub> ) [53]	1.644	1.356(90) [53]	1.783	1.454(45) [39, 53]	1.907	1.577(57) [39, 53]
$^{180}\text{Hf}$	0.463	1.441	1.510( $^{+0.182}$ <sub>-0.150</sub> )[53]	1.611	1.452(105) [53]	1.720	1.581(87) [40, 53]	1.811	1.536(80) [40, 53]
$^{182}\text{Hf}$	0.434	1.445	—	1.622	—	1.743	—	1.847	—
$^{184}\text{Hf}$	0.382	1.455	—	1.652	—	1.799	—	1.929	—
$^{170}\text{W}$ [36]	0.101	1.583	1.444(149)	1.957	1.524(119)	2.247	1.532(405)	2.476	1.371(324)

continued on next page

Table B – continued

Isotope	$r_\beta$	Transition ratios							
		$\frac{B(E2; 4_1^+ \rightarrow 2_1^+)}{B(E2; 2_1^+ \rightarrow 0_1^+)}$		$\frac{B(E2; 6_1^+ \rightarrow 4_1^+)}{B(E2; 2_1^+ \rightarrow 0_1^+)}$		$\frac{B(E2; 8_1^+ \rightarrow 6_1^+)}{B(E2; 2_1^+ \rightarrow 0_1^+)}$		$\frac{B(E2; 10_1^+ \rightarrow 8_1^+)}{B(E2; 2_1^+ \rightarrow 0_1^+)}$	
		CBS	Exp	CBS	Exp	CBS	Exp	CBS	Exp
$^{172}\text{W}$ [78]	0.157	1.555	1.433(164)	1.904	1.520(220)	2.182	1.696(230)	2.405	1.579(272)
$^{174}\text{W}$ [79]	0.285	1.487	1.741(146)	1.741	3.037(626)	1.951	1.778(252)	2.135	1.185(236)
$^{176}\text{W}$ [54]	0.287	1.486	1.518(81)	1.739	1.800(72)	1.948	1.253(149)	2.130	1.118( $^{+0.260}_{-0.178}$ )
$^{178}\text{W}$ [54]	0.321	1.473	1.442( $^{+0.089}_{-0.083}$ )	1.703	1.494( $^{+0.871}_{-0.417}$ )	1.888	—	2.053	—
$^{180}\text{W}$ [54]	0.334	1.468	1.447(63)	1.691	1.411( $^{+0.582}_{-0.321}$ )	1.867	—	2.025	—
$^{182}\text{W}$ [42]	0.427	1.446	1.440(76)	1.626	1.477(163)	1.750	1.536(134)	1.857	1.492(141)
$^{184}\text{W}$ [43]	0.395	1.452	1.386( $^{+0.046}_{-0.078}$ )	1.644	1.511(54)	1.783	1.544 (47)	1.907	1.578( $^{+0.095}_{-0.070}$ )
$^{186}\text{W}$ [44]	0.386	1.454	1.281( $^{+0.099}_{-0.091}$ )	1.649	1.610( $^{+0.135}_{-0.118}$ )	1.794	1.584( $^{+0.118}_{-0.109}$ )	1.922	1.352( $^{+0.161}_{-0.303}$ )
$^{188}\text{W}$	0.266	1.495	—	1.763	—	1.987	—	2.178	—
$^{176}\text{Os}$	0.098	1.584	—	1.959	—	2.249	—	2.478	—
$^{178}\text{Os}$	0.144	1.562	—	1.918	—	2.200	—	2.425	—
$^{180}\text{Os}$ [40]	0.203	1.528	1.362(229)	1.846	1.135(308)	2.106	—	2.319	—
$^{182}\text{Os}$ [55]	0.238	1.509	—	1.799	—	2.040	—	2.243	—
$^{184}\text{Os}$ [43]	0.322	1.472	1.406(402)	1.701	—	1.885	—	2.049	—
$^{186}\text{Os}$ [44]	0.295	1.483	1.442(81)	1.730	1.976(96)	1.933	1.410(81)	2.112	2.030(643)
$^{188}\text{Os}$ [45]	0.239	1.509	1.716(106)	1.798	1.781(106)	2.039	1.871(119)	2.241	2.387( $^{+0.311}_{-0.196}$ )
$^{190}\text{Os}$ [46]	0.130	1.569	1.358( $^{+0.075}_{-0.051}$ )	1.933	1.550(102)	2.218	1.867( $^{+0.305}_{-0.237}$ )	2.444	1.564( $^{+0.372}_{-0.304}$ )

Table C: Excitation energies (in keV) for even–even nuclei in the  $\beta$ -band (CBS), including intra-band CBS  $B(E2)$  ratios in the  $\beta$  band.

Isotope	$r_\beta$	CBS energies (keV)				CBS $B(E2)$ ratios	
		$E(0_\beta^+)$	$E(2_\beta^+)$	$E(4_\beta^+)$	$E(6_\beta^+)$	$\frac{B(E2; 4_\beta^+ \rightarrow 2_\beta^+)}{B(E2; 2_\beta^+ \rightarrow 0_\beta^+)}$	$\frac{B(E2; 6_\beta^+ \rightarrow 4_\beta^+)}{B(E2; 2_\beta^+ \rightarrow 0_\beta^+)}$
$^{122}\text{Ce}$	0.292	1560.27	1724.91	2106.97	2695.59	1.411	1.543
$^{124}\text{Ce}$	0.280	1531.83	1704.12	2103.02	2714.19	1.410	1.544
$^{126}\text{Ce}$	0.210	1390.07	1618.60	2132.16	2876.15	1.411	1.582
$^{128}\text{Ce}$	0.138	1336.69	1652.02	2307.36	3177.74	1.436	1.691
$^{150}\text{Ce}$	0.272	1013.52	1132.31	1406.83	1825.70	1.410	1.545
$^{152}\text{Ce}$	0.364	1292.51	1384.15	1598.19	1934.01	1.418	1.548
$^{154}\text{Ce}$	0.410	1530.94	1615.56	1813.34	2124.60	1.422	1.554
$^{128}\text{Nd}$	0.273	1420.43	1586.14	1969.20	2553.97	1.410	1.545
$^{130}\text{Nd}$	0.188	1212.41	1435.49	1928.25	2624.71	1.415	1.607
$^{150}\text{Nd}$	0.098	783.20	999.81	1422.56	1963.52	1.466	1.768
$^{152}\text{Nd}$	0.382	1257.41	1338.13	1526.75	1823.18	1.420	1.550
$^{154}\text{Nd}$	0.424	1513.46	1590.80	1771.57	2056.18	1.422	1.556
$^{156}\text{Nd}$	0.454	1684.64	1757.06	1926.31	2192.85	1.424	1.561
$^{158}\text{Nd}$	0.437	1515.39	1587.11	1754.73	2018.70	1.423	1.558
$^{132}\text{Sm}$	0.283	1444.96	1604.77	1975.01	2543.16	1.410	1.543
$^{152}\text{Sm}$	0.199	940.01	1103.89	1469.12	1991.67	1.412	1.594
$^{154}\text{Sm}$	0.363	1297.57	1390.27	1606.80	1946.46	1.418	1.547
$^{156}\text{Sm}$	0.443	1789.12	1870.99	2062.33	2363.66	1.423	1.559
$^{158}\text{Sm}$	0.460	1876.40	1954.46	2136.87	2424.15	1.425	1.561
$^{160}\text{Sm}$	0.457	1794.46	1870.31	2047.57	2326.73	1.424	1.561
$^{162}\text{Sm}$	0.448	1732.68	1809.97	1990.6	2275.06	1.424	1.560
$^{164}\text{Sm}$	0.394	1276.74	1353.71	1533.61	1816.53	1.421	1.552
$^{154}\text{Gd}$	0.203	964.93	1129.76	1498.22	2027.74	1.412	1.589
$^{156}\text{Gd}$	0.339	1260.60	1363.26	1602.78	1977.12	1.416	1.544
$^{158}\text{Gd}$	0.415	1625.50	1712.72	1916.58	2237.47	1.422	1.555
$^{160}\text{Gd}$	0.441	1764.97	1846.64	2037.51	2338.10	1.423	1.559
$^{162}\text{Gd}$	0.440	1670.68	1748.46	1930.24	2216.51	1.423	1.558
$^{164}\text{Gd}$	0.476	2054.21	2132.19	2314.41	2601.35	1.425	1.563
$^{166}\text{Gd}$	0.455	1759.34	1834.69	2010.78	2288.10	1.424	1.561
$^{156}\text{Dy}$	0.139	893.287	1102.88	1539.24	2119.57	1.565	1.924
$^{158}\text{Dy}$	0.306	1204.25	1321.98	1595.76	2019.89	1.413	1.542
$^{160}\text{Dy}$	0.368	1419.58	1518.06	1748.12	2109.21	1.418	1.548
$^{162}\text{Dy}$	0.416	1663.42	1752.12	1959.45	2285.81	1.422	1.555

continued on next page

Table C – continued

Isotope	$r_\beta$	CBS energies (keV)				CBS $B(E2)$ ratios	
		$E(0_\beta^+)$	$E(2_\beta^+)$	$E(4_\beta^+)$	$E(6_\beta^+)$	$\frac{B(E2; 4_\beta^+ \rightarrow 2_\beta^+)}{B(E2; 2_\beta^+ \rightarrow 0_\beta^+)}$	$\frac{B(E2; 6_\beta^+ \rightarrow 4_\beta^+)}{B(E2; 2_\beta^+ \rightarrow 0_\beta^+)}$
$^{164}\text{Dy}$	0.430	1624.37	1704.52	1891.86	2186.83	1.423	1.557
$^{166}\text{Dy}$	0.464	2020.17	2102.56	2295.09	2598.30	1.424	1.562
$^{168}\text{Dy}$	0.461	1954.52	2035.28	2223.98	2521.17	1.424	1.561
$^{170}\text{Dy}$	0.495	2231.32	2307.30	2484.82	2764.33	1.426	1.565
$^{160}\text{Er}$	0.233	1122.78	1285.58	1656.51	2206.51	1.409	1.562
$^{162}\text{Er}$	0.323	1348.14	1467.90	1746.97	2181.58	1.414	1.542
$^{164}\text{Er}$	0.382	1592.79	1695.34	1934.95	2311.51	1.420	1.550
$^{166}\text{Er}$	0.387	1447.93	1538.43	1749.92	2082.40	1.420	1.551
$^{168}\text{Er}$	0.463	2094.64	2180.52	2381.21	2697.28	1.425	1.562
$^{170}\text{Er}$	0.467	2107.92	2192.24	2389.27	2699.56	1.425	1.562
$^{172}\text{Er}$	0.471	2106.03	2188.57	2381.43	2685.15	1.425	1.562
$^{162}\text{Yb}$	0.036	958.60	1261.11	1809.19	2496.81	1.505	1.840
$^{164}\text{Yb}$	0.229	1097.52	1260.63	1631.39	2178.84	1.409	1.565
$^{166}\text{Yb}$	0.323	1348.60	1468.65	1748.37	2183.96	1.414	1.543
$^{168}\text{Yb}$	0.354	1344.84	1445.54	1680.67	2049.11	1.418	1.546
$^{170}\text{Yb}$	0.419	1761.96	1854.45	2070.63	2410.95	1.422	1.556
$^{172}\text{Yb}$	0.454	1968.90	2053.82	2252.28	2564.82	1.424	1.560
$^{174}\text{Yb}$	0.462	2001.93	2084.23	2276.53	2579.39	1.425	1.561
$^{176}\text{Yb}$	0.453	2046.07	2134.91	2342.54	2669.51	1.424	1.560
$^{178}\text{Yb}$	0.509	2985.53	3072.70	3276.28	3596.73	1.426	1.567
$^{166}\text{Hf}$	0.136	1030.19	1275.49	1783.74	2457.16	1.438	1.695
$^{168}\text{Hf}$	0.228	1092.53	1255.43	1625.63	2171.92	1.409	1.566
$^{170}\text{Hf}$	0.274	1077.72	1202.93	1492.40	1934.50	1.410	1.545
$^{172}\text{Hf}$	0.339	1351.58	1462.00	1719.58	2122.14	1.416	1.544
$^{174}\text{Hf}$	0.364	1454.21	1557.74	1799.55	2178.89	1.418	1.547
$^{176}\text{Hf}$	0.392	1622.23	1720.80	1951.16	2313.43	1.420	1.552
$^{178}\text{Hf}$	0.395	1738.57	1842.76	2086.26	2469.24	1.421	1.552
$^{180}\text{Hf}$	0.463	2450.97	2551.22	2785.47	3154.38	1.425	1.561
$^{182}\text{Hf}$	0.434	2207.44	2313.66	2561.94	2952.89	1.423	1.558
$^{184}\text{Hf}$	0.382	1863.02	1982.95	2263.19	2703.60	1.420	1.550
$^{170}\text{W}$	0.101	951.74	1212.73	1724.12	2379.65	1.464	1.763
$^{172}\text{W}$	0.157	867.83	1054.95	1454.25	1996.93	1.426	1.656
$^{174}\text{W}$	0.285	1221.44	1355.23	1665.28	2141.48	1.411	1.543

continued on next page

Table C – continued

Isotope	$r_\beta$	CBS energies (keV)				CBS $B(E2)$ ratios	
		$E(0_\beta^+)$	$E(2_\beta^+)$	$E(4_\beta^+)$	$E(6_\beta^+)$	$\frac{B(E2; 4_\beta^+ \rightarrow 2_\beta^+)}{B(E2; 2_\beta^+ \rightarrow 0_\beta^+)}$	$\frac{B(E2; 6_\beta^+ \rightarrow 4_\beta^+)}{B(E2; 2_\beta^+ \rightarrow 0_\beta^+)}$
$^{176}\text{W}$	0.287	1229.41	1362.63	1671.48	2146.28	1.411	1.543
$^{178}\text{W}$	0.321	1390.55	1515.58	1806.87	2260.25	1.414	1.542
$^{180}\text{W}$	0.334	1452.86	1574.86	1859.40	2303.61	1.415	1.544
$^{182}\text{W}$	0.427	2174.47	2283.55	2538.50	2939.92	1.423	1.557
$^{184}\text{W}$	0.395	2059.69	2183.07	2471.43	2924.98	1.420	1.552
$^{186}\text{W}$	0.386	2134.76	2269.18	2583.29	3077.06	1.420	1.550
$^{188}\text{W}$	0.266	1432.05	1605.82	2006.73	2616.13	1.409	1.547
$^{176}\text{Os}$	0.098	805.80	1028.78	1463.86	2020.52	1.466	1.768
$^{178}\text{Os}$	0.144	887.63	1090.98	1517.52	2088.27	1.433	1.679
$^{180}\text{Os}$	0.203	1064.15	1245.49	1651.02	2234.10	1.411	1.589
$^{182}\text{Os}$	0.238	1177.19	1343.54	1723.42	2289.04	1.409	1.559
$^{184}\text{Os}$	0.322	1561.94	1701.30	2026.00	2531.57	1.414	1.543
$^{186}\text{Os}$	0.295	1576.73	1740.27	2119.98	2705.77	1.412	1.542
$^{188}\text{Os}$	0.239	1408.18	1606.45	2059.36	2734.11	1.409	1.559
$^{190}\text{Os}$	0.130	1199.58	1492.31	2093.73	2885.73	1.441	1.706